arXiv:2012.01540v1 [stat.ME] 2 Dec 2020

# Robust functional principal components for sparse longitudinal data

Graciela Boente[1] and Matías Salibián-Barrera[2]

[1]Universidad de Buenos Aires and CONICET, Argentina ,
gboente@dm.uba.ar
[2]University of British Columbia, Canada, matias@stat.ubc.ca

December 9, 2021

**Abstract**

In this paper we review existing methods for robust functional principal component analysis (FPCA) and propose a new method for FPCA that can be applied to longitudinal data where only a few observations per trajectory are available. This method is robust against the presence of atypical observations, and can also be used to derive a new non-robust FPCA approach for sparsely observed functional data. We use local regression to estimate the values of the covariance function, taking advantage of the fact that for elliptically distributed random vectors the conditional location parameter of some of its components given others is a linear function of the conditioning set. This observation allows us to obtain robust FPCA estimators by using robust local regression methods. The finite sample performance of our proposal is explored through a simulation study that shows that, as expected, the robust method outperforms existing alternatives when the data are contaminated. Furthermore, we also see that for samples that do not contain outliers the non-robust variant of our proposal compares favourably to the existing alternative in the literature. A real data example is also presented.

AMS Subject Classification 2000: MSC 62F35, MSC 62H25.
Key words and phrases: Functional data analysis; Principal components; Robust estimation; Sparse data

# 1 Introduction

Functional Data Analysis refers to a collection of statistical models that apply to data that can be naturally represented as observations taken from (mostly unobserved) underlying functions. Instead of simply treating the data as vectors, models with a functional structure naturally incorporate into the analysis important characteristics of the random process generating the observations, such as smoothness. Functional models represent the partially observed functions as random elements on a functional space, such as $L^2(\mathcal{I})$, with $\mathcal{I} \subset \mathbb{R}$ a finite interval. Given the infinite dimension of this type of sample spaces, some form of dimension reduction or regularization is typically required. Functional Principal Components Analysis (FPCA) is a commonly used approach to obtain optimal lower-dimensional representations of the observations (Boente *et al.*, [7]). Moreover, FPCA can also be used to describe the main characteristics of the process generating the functions, similarly to what is done in the finite-dimensional case with the interpretation of PCA loadings. Specifically, the trajectories of each subject can be represented by their coefficients (scores) on a few elements of the basis of eigenfunctions (see for instance, Ramsay and Silverman [47] and Hall and Horowitz [26].) Other bases can also be used to represent the trajectories, e.g. a sufficiently rich $B$-splines basis (James *et al.*, [36]).

In this paper, we study the problem of reliably estimating the principal functions when the data may contain a small proportion of atypical observations. It is well-known that, similarly to what happens in the finite dimensional case, most FPCA methods can be seriously affected in such a situation. The outliers need not be "extreme" data points, but might consist of curves that behave differently from the others, or that display a persistent behaviour either in shift, amplitude and/or shape (see, e.g., Hubert *et al.* [32]).

Robust FPCA methods in the literature can be classified in three groups, depending on the specific property of principal components on which they focus. Some of them rely on performing the eigenanalysis of a robust estimator of the covariance or scatter operator. Others estimate the principal functions by searching for directions that maximize a robust estimator of the spread or scale of the corresponding projections. A third group of robust methods estimate the principal subspaces by minimizing a robust measure of the reconstruction error (the discrepancy between the observations and their orthogonal projections on the eigenspace). A more detailed discussion can be found in Section 2 below.

Most functional data analysis methods assume that each trajectory is observed on a relatively fine grid of points, often equally spaced. The corresponding ap-

proaches to analyze such functional data can be found, for instance, in Ramsay and Silverman [47], Ferraty and Vieu [19] and Ferraty and Romain [18]. Recent reviews of functional data analysis methods include: Horváth and Kokoszka [29], Hsing and Eubank [30], Cuevas [13], Goia and Vieu [25], and Wang *et al.* [53].

To the best of our knowledge, most of the robust FPCA methods proposed in the literature also require that the curves be observed in a relatively dense grid. However, there are many applications in which trajectories are measured only a few times for each sampling unit. Such longitudinal data sets with only a few available observations per curve (possibly recorded at irregular intervals), are relatively common in applications, and in many cases it is sensible to consider an underlying functional structure (of smooth trajectories, for example). Only a few FPCA methods exist in the literature for this type of data (see for example, James *et al.* [36], Yao *et al.* [56] and Li and Hsing [39]).

The approach of James *et al.*, [36] consists of assuming a finite-dimensional expansion for the underlying random process (i.e. a Karhunen-Loeve expansion with only finitely many terms), and approximating the mean function and eigenfunctions with splines. An alternative proposal was given by Yao *et al.* [56] (see also Staniswalis and Lee [51]). It consists of estimating the covariance function using a bivariate smoother over the cross-products of the available observations. In this way, information about the covariance function of the process at different points is "borrowed" from different curves. Principal directions are constructed from the estimated covariance function, and scores are estimated using best linear predictors. Similarly, Li and Hsing [39] estimate the mean and covariance functions with local linear smoothers, but use weights to ensure that the effect that each curve has on the optimizers is not overly affected by the number of points at which they were observed.

To construct robust FPCA estimators, Gervini [24] modified the reduced rank proposal of James *et al.*, [36] assuming that the finite-dimensional standardized scores and the measurement errors have a joint multivariate Student's T distribution. The resulting estimators for the centre function and eigenfunctions are Fisher-consistent. A related method using $MM$-estimators for the basis coefficients and scores has been recently proposed by Maronna [43].

An intuitively straightforward approach to obtain a robust version of the method proposed by Yao *et al.* [56] would be to replace the bivariate smoother of the cross-products with a robust alternative. However, the regression approach of Staniswalis and Lee [51], and Yao *et al.* [56] works because the smoother estimates the conditional mean of the cross-products, which is the covariance function. The main

challenge with using a robust smoother in this setting is that, to the best of our knowledge, there are no robust estimators for the expected value of asymmetrically distributed random variables without imposing distributional assumptions. Hence, a robust smoother of the cross-products will typically not be able to estimate the covariance function.

In this paper, we provide an alternative approach to obtain a robust estimate of the covariance function in the case of sparsely observed functional (longitudinal) data. Furthermore, this proposal can naturally be adapted to offer another way to perform FPCA for longitudinal data in the settings considered by Yao *et al.* [56]. Our proposal is based on a well-known property of the conditional distribution of elliptically distributed random vectors: the conditional location parameter of one of its components given others is a linear function of the set of conditioning values. We first show that for an elliptically distributed random process, the vector of its values at a fixed set of points has a multivariate elliptical distribution. Combining this property with the previous one, we propose to use a robust local regression method to estimate the values of the covariance function when outliers may be present in the data. Our approach can also be used with a non-robust local regression method, and our numerical experiments show that this method compares favourably to that of Yao *et al.* [56].

The rest of the paper is organized as follows. In Section 2 we review previously proposed robust FPCA methods which are applicable when either the entire trajectories were observed, or they were recorded on a dense grid of points. Section 3 describes our robust estimator of the principal directions for sparsely recorded data. We discuss the results of our numerical experiments studying the robustness and finite sample performance of the different methods in Section 4. An illustration is discussed in Section 5, while Section 6 contains a discussion and further recommendations.

## 2 Robust methods for FPCA

As mentioned in the Introduction, atypical observations in a functional setting need not be "extreme" points and may occur in several different ways. Often they correspond to individuals that follow a different pattern than that of the majority of the data. The detection of such outliers is generally a difficult problem, and some proposals exist in the literature. Among others, we can mention the procedures described in Febrero *et al.* [15, 16], Hyndman and Ullah [35], Hyndman and Shang [34], Sawant *et al.* [48], and Sun and Genton [52].

In this paper we are concerned with methods that do not require the preliminary detection of potential atypical observations in the data. We need to introduce some notation and definitions. Although we are motivated by situations where data that can be represented as random elements $X$ on a functional space, like $L^2(\mathcal{I})$, with $\mathcal{I} \subset \mathbb{R}$ a finite interval, most of our discussion can be generalized to the case where $X$ is a random element on an arbitrary separable Hilbert space $\mathcal{H}$. Denote the corresponding inner product and norm with $\langle \cdot, \cdot \rangle$ and $\|u\| = \langle u, u \rangle^{1/2}$, respectively. In classical FPCA one assumes that $\mathbb{E}\|X\|^2 < \infty$, which ensures the existence of the mean and the covariance operator (denoted by $\mu_X = \mathbb{E}(X)$ and $\Gamma_X : \mathcal{H} \to \mathcal{H}$, respectively). The covariance operator can be written as $\Gamma_X = \mathbb{E}\{(X - \mu_X) \otimes (X - \mu_X)\}$, where $\otimes$ denotes the tensor product on $\mathcal{H}$, i.e., the operator $u \otimes v : \mathcal{H} \to \mathcal{H}$ given by $(u \otimes v)w = \langle v, w \rangle u$ for $w \in \mathcal{H}$. When $\mathcal{H} = L^2(\mathcal{I})$, the mean function $\mu_X$ satisfies $\mu_X(t) = E(X(t))$ for $t \in \mathcal{I}$, and the covariance operator $\Gamma_X$ is associated with a symmetric, non-negative definite covariance function $\gamma_X : \mathcal{I} \times \mathcal{I} \to \mathbb{R}$ such that $\int_{\mathcal{I}} \int_{\mathcal{I}} \gamma_X^2(t, s)\, ds\, dt < \infty$, as follows $(\Gamma_X f)(t) = \int_{\mathcal{I}} \gamma_X(s, t)\, f(s)\, ds$.

The covariance operator $\Gamma_X$ is linear, self-adjoint, continuous, and Hilbert-Schmidt. Hilbert-Schmidt operators have a countable number of eigenvalues, all of them real when the operator is self-adjoint. Let $\{\phi_\ell : \ell \geq 1\}$ be the eigenfunctions of $\Gamma_X$ associated with its eigenvalues $\lambda_1 \geq \lambda_2 \geq \cdots$ in decreasing order. The Karhunen-Loève expansion of the process $X$ is given by the representation $X = \mu_X + \sum_{\ell=1}^{\infty} \xi_\ell\, \phi_\ell$, where the convergence of the series is in mean square norm, that is, $\lim_{q \to \infty} \mathbb{E}\|X - \mu_X - \sum_{\ell=1}^{q} \xi_\ell\, \phi_\ell\|^2 = 0$. The random variables $\{\xi_\ell : \ell \geq 1\}$ are the coordinates of $X - \mu_X$ on the basis $\{\phi_\ell : \ell \geq 1\}$, that is, $\xi_\ell = \langle X - \mu_X, \phi_\ell \rangle$. Note that $\mathbb{E}(\xi_\ell) = 0$, $\mathbb{E}(\xi_\ell^2) = \lambda_\ell$, and $\mathbb{E}(\xi_\ell \xi_s) = 0$ for $\ell \neq s$.

In multivariate analysis, elliptical distributions provide an important framework for the development of robust principal component procedures. Elliptical processes play a similar role for the development of robust FPCA methods, allowing for random elements that may not have finite second moments. Given $\mu \in \mathcal{H}$, usually known as the location parameter, and $\Gamma$, a self-adjoint, positive semi-definite and Hilbert-Schmidt operator on $\mathcal{H}$ (the scatter operator), we say that the process $X$ has an elliptical distribution $\mathcal{E}(\mu, \Gamma, \varphi)$, if for any linear bounded operator $A : \mathcal{H} \to \mathbb{R}^d$ the random vector $AX$ has a multivariate elliptical distribution $\mathcal{E}_d(A\mu, A\Gamma A^*, \varphi)$, where $A^*$ denotes the adjoint operator of $A$ and $\varphi$ stands for the characteristic generator. It is easy to see that Gaussian processes satisfy the above definition with $\varphi(a) = \exp(-a/2)$. When second moments exist, the mean of $X$ is $\mu$ and the covariance operator is proportional to $\Gamma$, i.e., $\mu_X = \mu$ and $\Gamma_X = \alpha\, \Gamma$ for some $\alpha > 0$ (see Lemma 2.2 in Bali and Boente [1]). As noted in Boente *et al.* [7], the scatter operator $\Gamma$ is confounded with the function $\varphi$ meaning that for any $c > 0$,

$\mathcal{E}(\mu, \Gamma, \varphi) \sim \mathcal{E}(\mu, c\,\Gamma, \varphi_c)$ where $\varphi_c(w) = \varphi(w/c)$. For that reason, without loss of generality, when second moments exist, we will assume that $\Gamma_X = \Gamma$. We refer the interested reader to Bali and Boente [1] and Boente *et al.* [7].

Like their finite-dimensional counterparts, functional principal components satisfy the following three equivalent properties:

- **Property 1:** The first principal directions correspond to the eigenfunctions of the covariance operator $\Gamma_X$ associated with its largest eigenvalues.
- **Property 2:** The first principal direction maximizes $\textsc{Var}\left(\langle \alpha, X \rangle\right)$ over the unit sphere $\mathcal{S} = \{\alpha : \|\alpha\| = 1\}$, and subsequent ones solve the same optimization problem subject to the condition that $\alpha$ be orthogonal to all the previous principal directions.
- **Property 3:** The first $q$ principal directions provide the best $q$-dimensional linear approximation to the random element in terms of mean squared error. Specifically, let $\pi(x, \mathcal{L})$ denote the orthogonal projection of $x \in \mathcal{H}$ onto an arbitrary $q$-dimensional closed linear space $\mathcal{L}$, and $\mathcal{L}_0$ be the linear space spanned by the eigenfunctions of $\Gamma_X$ associated with its $q$ largest eigenvalues $\lambda_1 \geq \cdots \geq \lambda_q$. If $\lambda_q > \lambda_{q+1}$, then we have $\mathbb{E}(\|(X-\mu_X)-\pi((X-\mu_X), \mathcal{L}_0)\|^2) \leq \mathbb{E}(\|(X-\mu_X)-\pi((X-\mu_X), \mathcal{L})\|^2)$.

As mentioned in the Introduction, robust functional principal components estimators proposed in the literature can be classified in three groups, according to the property on which they focus. The first approach is based on obtaining a robust counterpart to the sample covariance operator, and use its eigenfunctions to perform robust FPCA. The second group consists of methods that sequentially search for directions that maximize a robust estimator of the spread or scale of the projections. The last class of robust FPCA methods estimates principal subspaces by searching the closed linear subspace $\mathcal{L}$ that minimizes a robust measure of scale of the reconstruction error $\|(X-\mu)-\pi((X-\mu), \mathcal{L})\|$ (the distance between the data and their orthogonal projections onto the subspace), where $\mu$ denotes a location parameter.

In the rest of this section we review the robust FPCA methods that are available in each of these three groups. Our proposal for the case of sparsely observed trajectories is discussed in the next Section.

## 2.1 Methods based on Property 1

Probably the earliest robust functional principal components estimators in the literature are those introduced in Locantore *et al.* [40]. They proposed the so-called spherical principal components, which were further studied in Gervini [23] and Boente *et al.* [5]. The basic idea is to control potential outliers in the data by normalizing the observations (forcing all curves to lie on the unit sphere). Formally, given a centre $\mu \in \mathcal{H}$, the spatial or sign covariance operator of $X$ centered at $\mu$ is defined as

$$\Gamma^{\mathrm{S}}(\mu) \;=\; \mathbb{E}\left[\left(\frac{X-\mu}{\|X-\mu\|}\right)\otimes\left(\frac{X-\mu}{\|X-\mu\|}\right)\right], \tag{1}$$

which can be estimated through its sample version:

$$\widehat{\Gamma}^{\mathrm{S}}(\mu) \;=\; \frac{1}{n}\sum_{i=1}^{n}\left(\frac{X_i-\mu}{\|X_i-\mu\|}\right)\otimes\left(\frac{X_i-\mu}{\|X_i-\mu\|}\right).$$

Several location parameters (centres) have been considered in the literature. When using the sign covariance operator (1) the standard choice for the centre $\mu$ is the functional spatial or geometric median: $\mu_{\mathrm{GM}} = \mathrm{argmin}_{u\in\mathcal{H}}\,\mathbb{E}\,(\|X-u\|-\|X\|)$ (see Locantore *et al.* [40] and Gervini [23]). It can be estimated by its sample version $\widehat{\mu}_{\mathrm{GM}} = \mathrm{argmin}_{u\in\mathcal{H}}\sum_{i=1}^{n}\|X-u\|$ leading to the usual spatial operator estimator $\widehat{\Gamma}^{\mathrm{S}}(\widehat{\mu}_{\mathrm{GM}})$. The spherical principal direction estimators correspond to its eigenfunctions. We refer to Gervini [23] and Cardot *et al.* [9] for consistency results of the geometric median estimator and to Boente *et al.* [5] for results regarding the asymptotic distribution of $\widehat{\Gamma}^{\mathrm{S}}(\widehat{\mu})$ and the spherical principal directions. Other robust location estimators for $\mu$ above may be considered. For example, the $\alpha$-trimmed mean introduced in Fraiman and Muñiz [22], the deepest point (e.g. Cuevas [13], Cuevas *et al.* [14] and López-Pintado and Romo [41]) and the $M$-location estimator in Sinova *et al.* [50].

In addition to being easy to compute, another appealing property of the spherical principal directions is that, under certain conditions they can be shown to be Fisher-consistent. Specifically, assume that either $X$ has an elliptical distribution, as defined above, with location $\mu$ and scatter operator $\Gamma$, or that $X$ has a finite-rank representation $X = \mu + \sum_{\ell=1}^{q}\lambda_\ell^{1/2} f_\ell\,\phi_\ell$, where the random vector $(f_1,\ldots,f_q)$ has exchangeable symmetric marginal distributions (in this case, we denote $\Gamma = \sum_{j=1}^{q}\lambda_j\,\phi_j\otimes\phi_j$). Then, the eigenfunctions of $\Gamma^{\mathrm{S}}(\mu)$ are the same as those of $\Gamma$ and in the same order (see Boente *et al.* [7] and Gervini [23]).

Other robust scatter operator estimators have been proposed in the literature. For example, the $\rho$-scatter operator of Kraus and Panaretos [37], and the geometric

median covariation studied in Cardot and Godichon-Baggioni [10]. However, the eigenfunctions of these operators are not guaranteed to remain in the same order as those of the true covariance operator when the latter exists, or of the true scatter operator for elliptical processes.

Sawant *et al.* [48] proposed to estimate the principal directions and their size indirectly using the following approach. Ramsay and Silverman [47] showed that if the observed trajectories $X_i$ and the eigenfunctions $\phi_\ell$ of the covariance operator are represented on a common known basis (e.g. splines or Fourier), then FPCA can be performed using standard finite-dimensional PCA on the matrix of coefficients representing the observations on the chosen basis. The robust version of this procedure in Sawant *et al.* [48] consists of replacing the PCA step above with a robust PCA alternative. In particular, they used ROBPCA (Hubert *et al.* [31]) and BACONPCA (Billor *et al.* [3]).

## 2.2 Methods based on Property 2

Proposals to perform robust FPCA relying on Property 2 above are typically referred to as projection-pursuit approaches. Hyndman and Ullah [35] discussed a robust projection-pursuit method applied to smoothed observed trajectories. Bali *et al.* [2] generalized this approach combining it with penalization and basis reduction. In order to impose smoothness on the estimated eigenfunctions, regularization is included via a penalization operator. Consider the subset $\mathcal{H}_{\mathrm{S}}$, of *smooth elements* of $\mathcal{H}$ and $D : \mathcal{H}_{\mathrm{S}} \to \mathcal{H}$ a linear operator, usually called the "differentiator", since when $\mathcal{H} = L^2(\mathcal{I})$ one typically takes $D\alpha = \alpha''$. Associated with $D$ one can construct the following symmetric positive semi-definite bilinear form $\lceil \cdot, \cdot \rceil : \mathcal{H}_{\mathrm{S}} \times \mathcal{H}_{\mathrm{S}} \to \mathbb{R}$, where $\lceil \alpha, \beta \rceil = \langle D\alpha, D\beta \rangle$, and the functional $\Psi : \mathcal{H}_{\mathrm{S}} \to \mathbb{R}$ as $\Psi(\alpha) = \lceil \alpha, \alpha \rceil$. Finally, a penalized inner product is defined as $\langle \alpha, \beta \rangle_\tau = \langle \alpha, \beta \rangle + \tau \lceil \alpha, \beta \rceil$, and the associated norm is $\|\alpha\|_\tau^2 = \|\alpha\|^2 + \tau \Psi(\alpha)$.

Let $s_n(\alpha)$ be a robust univariate scale estimator $\sigma_n$ (e.g. an M-scale estimator) computed on the sample projections $\langle \alpha, X_1 \rangle, \ldots, \langle \alpha, X_n \rangle$. The intuitive idea is to estimate the first principal direction as the element $\alpha$ that maximizes $s_n^2(\alpha) - \rho\Psi(\alpha)$, over the unit sphere $\{\|\alpha\|_\tau = 1\} \subset \mathcal{H}$. In addition, Bali *et al.* [2] used a sieves approach to approximate the elements of $\mathcal{H}$ with an increasing sequence of known bases (e.g. splines). Formally, let $\{\delta_i\}_{i \geq 1}$ be a basis of $\mathcal{H}$, and $\mathcal{H}_{p_n}$ the linear space spanned by $\delta_1, \ldots, \delta_{p_n}$, with $p_n \to \infty$ as $n \to \infty$. The robust projection-pursuit estimator for the first principal direction in Bali *et al.* [2] is given by

$$\widehat{\phi}_1 = \underset{\alpha \in \mathcal{H}_{p_n}, \|\alpha\|_\tau = 1}{\operatorname{argmax}} \left\{ s_n^2(\alpha) - \rho\Psi(\alpha) \right\} .$$

The other principal directions are defined sequentially adding the condition that they be orthogonal to the previous ones with respect to the inner product $\langle \cdot, \cdot \rangle_\tau$. Bali *et al.* [2] showed that the estimators are qualitative robust. Furthermore, the procedure is Fisher-consistent when the robust univariate scale estimator $\sigma_n$ is the empirical version of a functional $\sigma_{\text{ROB}}$ such that there exist a constant $c > 0$ and a self-adjoint, positive semidefinite and Hilbert-Schmidt operator $\Gamma_0$ satisfying $\sigma^2_{\text{ROB}}(P[\alpha]) = c \langle \alpha, \Gamma_0 \alpha \rangle$ for all $\alpha \in \mathcal{H}$, where $P[\alpha]$ stands for the distribution of $\langle \alpha, X \rangle$. This condition is satisfied when $X$ has an elliptical distribution.

Note that the approaches described here and in Section 2.1 require that one is able to compute or approximate well the norms $\|X_i - \mu\|$ and inner products $\langle \alpha, X_i \rangle$. For example, when $\mathcal{H} = L^2(\mathcal{I})$ this typically means that the trajectories need to have been observed over a relatively dense grid of points. When the data are measured sparsely (and only a few points per trajectory are available) these methods become infeasible.

### 2.3 Methods based on Property 3

The last group of robust FPCA methods estimate the eigenspaces directly, for example by minimizing a robust measure of the distance between the observations and their orthogonal projections on finite-dimensional subspaces. Lee *et al.* [38] proposed a sequential algorithm fitting linear spaces of dimension 1 to the observed data. Their proposal assumes that all trajectories $X_i$, $1 \leq i \leq n$, were observed on a common grid $t_1, \ldots, t_m$. The goal is to find a smooth function $v$ and a vector $\mathbf{a} = (a_1, \ldots, a_n)^\top$ that minimize the size of the residuals $X_i(t_j) - a_i v(t_j)$. Because of the potential presence of outliers, the method uses a bounded loss function $\rho$. Given an initial estimator for $v$, let $a_i = \sum_{j=1}^m X_i(t_j) v(t_j)$, $1 \leq i \leq n$, and for each $j = 1, \ldots, m$, let $\widehat{\sigma}_j$ be a robust scale estimator of the residuals $X_i(t_j) - a_i v(t_j)$, $1 \leq i \leq n$. The estimators for $v$ and $\mathbf{a}$ are defined as the minimizers of

$$\sum_{i=1}^{n} \sum_{j=1}^{m} \widehat{\sigma}_j^2 \rho \left( \frac{X_i(t_j) - a_i\, v(t_j)}{\widehat{\sigma}_j} \right) + \frac{\lambda}{2} \int \left[ v''(t) \right]^2 dt \,,$$

subject to the constraint $\int v^2(t)\, dt = 1$, where $\lambda > 0$ is a user-chosen regularization parameter. This problem can be solved iteratively as follows. Given $\mathbf{a} = (a_1, \ldots, a_n)$ let $\phi_{\mathbf{a}}$ be the minimizer of the objective function above, which can be obtained using iterative reweighted penalized least-squares, and given $\phi_{\mathbf{a}}$, the entries of $\mathbf{a}$ are the projections of each trajectory along the direction $\phi_{\mathbf{a}}$: $a_i = \sum_{j=1}^m X_i(t_j) \phi_{\mathbf{a}}(t_j)$, $1 \leq i \leq n$. These steps are then iterated until convergence. Once the first principal direction $\widehat{\phi}_1$ is obtained, we can compute the corresponding estimated scores

$\widehat{\xi}_{i,1} = \sum_{j=1}^{m} X_i(t_j)\widehat{\phi}_1(t_j)$. The other estimated principal directions are computed sequentially as follows: assume that $\widehat{\phi}_s$, $s = 1, \ldots, \ell - 1$, are estimators of the first $\ell - 1$ principal directions, then, the $\ell-$th principal direction and the related scores are computed applying the previous procedure to $X(t_j) - \sum_{s=1}^{\ell-1} \widehat{\xi}_{i,s}\widehat{\phi}_s(t_j)$. Lee *et al.* [38] also discussed a data-dependent and resistant procedure to select $\lambda$.

In some applications each curve $X_i$ may be observed on a different (but dense) grid, and in that case we can, in principle, proceed as recommended in Ramsay and Silverman [47], namely: smooth each curve $X_i$ and apply the method above to the values of the smoothed trajectories on a fixed grid. A drawback of this strategy is that the errors introduced by the data smoothing step cannot be included easily in the analysis.

A different approach to estimate functional principal subspaces is as follows. Assume that each trajectory is observed on a dense grid of points (that may be specific to each curve), and let $\{\delta_i\}_{i\geq 1}$ be an orthonormal basis of $\mathcal{H}$. The basic idea is to identify each curve $X_i$ with the vector of its coefficients on a finite-dimensional basis, apply a robust multivariate method to estimate principal subspaces in this finite-dimensional space, and then map the results back to $\mathcal{H}$. Specifically, fix $p_n$, the basis size, and let $x_{ij} = \langle X_i, \delta_j \rangle$ be the coefficient of the $i$-th trajectory on the $j$-th element of the basis, $1 \leq j \leq p_n$. The grids where each $X_i$ are observed need to be sufficiently dense so that these inner products can be approximated well using finite Riemman sums. For each $1 \leq i \leq n$, let $\mathbf{x}_i$ be the vector of coefficients of $X_i$ on the basis $\{\delta_j\}_{1\leq j\leq p_n}$: $\mathbf{x}_i = (x_{i1}, \ldots, x_{ip_n})^{\mathrm{T}}$. We can now apply robust multivariate methods on the sample $\mathbf{x}_1, \ldots, \mathbf{x}_n$ to estimate a $q$ dimensional principal subspace $\widehat{\mathcal{L}} \subset \mathbb{R}^{p_n}$. Once the principal subspace $\widehat{\mathcal{L}}$ is found, the functional principal direction estimators can be reconstructed by "mapping back" the results in $\mathbb{R}^{p_n}$ onto $\mathcal{H}$. To fix ideas, let $\widehat{\mathbf{b}}^{(1)}, \ldots, \widehat{\mathbf{b}}^{(q)}$ be an orthonormal basis for $\widehat{\mathcal{L}}$ and let $\widehat{\mathbf{x}}_i = \widehat{\boldsymbol{\mu}} + \sum_{\ell=1}^{q} \widehat{a}_{i\ell}\widehat{\mathbf{b}}^{(\ell)}$ be the $q$-dimensional approximation to $\mathbf{x}_i$, where $\widehat{\boldsymbol{\mu}} = (\widehat{\mu}_1, \ldots, \widehat{\mu}_p)^{\mathrm{T}}$. The functional location parameter can be reconstructed as $\widehat{\mu} = \sum_{j=1}^{p_n} \widehat{\mu}_j\delta_j$, while the $q$-dimensional principal direction basis in $\mathcal{H}$ is $\widehat{\phi}_\ell = \sum_{j=1}^{p_n} \widehat{b}_{\ell j}\delta_j / \| \sum_{j=1}^{p_n} \widehat{b}_{\ell j}\delta_j \|$, for $1 \leq \ell \leq q$. Furthermore, the "fitted values" in $\mathcal{H}$ are $\widehat{X}_i = \widehat{\mu} + \sum_{\ell=1}^{q} \widehat{a}_{i\ell}\widehat{\phi}_\ell$.

The proposals of Boente and Salibian-Barrera [6] and Cevallos-Valdiviezo [11] are variants of this approach that differ on how the principal subspace $\widehat{\mathcal{L}} \subset \mathbb{R}^{p_n}$ and its orthonormal basis are estimated. Let $\mathbf{B} = \left(\mathbf{b}^{(1)}, \ldots, \mathbf{b}^{(q)}\right) \in \mathbb{R}^{p_n \times q}$ and $\mathbf{b}_j^{\mathrm{T}}$ the $j$-th row of $\mathbf{B}$. For a given $\boldsymbol{\mu} \in \mathbb{R}^{p_n}$ and $\mathbf{a}_i \in \mathbb{R}^q$, the corresponding "fitted values" are $\widehat{\mathbf{x}}_i(\boldsymbol{\mu}, \mathbf{B}, \mathbf{A}) = \boldsymbol{\mu} + \mathbf{B}\mathbf{a}_i$, where $\mathbf{a}_i$ are the columns of the matrix $\mathbf{A} \in \mathbb{R}^{q \times p_n}$.

Boente and Salibian-Barrera [6] estimated the principal subspace minimizing $\sum_{j=1}^{p} \widehat{\sigma}_j^2(\boldsymbol{\mu}, \mathbf{B}, \mathbf{A})$, where $\widehat{\sigma}_j(\boldsymbol{\mu}, \mathbf{B}, \mathbf{A})$ is a robust scale of the $j$-th coordinate of the

residual vectors $\mathbf{r}_i = \mathbf{x}_i - \widehat{\mathbf{x}}_i(\boldsymbol{\mu}, \mathbf{B}, \mathbf{A})$, $1 \leq i \leq n$. Although in principle one can use any robust scale estimator, Boente and Salibian-Barrera [6] discussed in detail the case of $M$-scale estimators (see Maronna *et al.* [42]), for which an iterative algorithm can be derived. Cevallos-Valdiviezo [11] proposed using a multivariate $S$-estimator for PCA, minimizing $\widehat{\sigma}(\boldsymbol{\mu}, \mathbf{B}, \mathbf{A})$, where $\widehat{\sigma}(\boldsymbol{\mu}, \mathbf{B}, \mathbf{A})$ is a robust scale of the distances $d_i(\mathbf{A}, \mathbf{B}, \boldsymbol{\mu}) = \|\mathbf{x}_i - \widehat{\mathbf{x}}_i(\boldsymbol{\mu}, \mathbf{B}, \mathbf{A})\|$, using $M$-scale and least-trimmed scale estimators. All these proposals are Fisher-consistent for elliptically distributed random processes.

# 3 FPCA for longitudinal (sparse) data

In this section we describe a new robust FPCA method that is applicable to the case where few observations per trajectory may be available. Moreover, when robustness is not a concern, our proposal results in a novel method for non-robust FPCA that compares favourably with existing methods in the literature.

## 3.1 Model

We will assume the following framework. Let $\{X(t) : t \in \mathcal{I}\}$ be a stochastic process defined on a probability space $(\Omega, \mathcal{A}, \mathbb{P})$ with continuous trajectories, where $\mathcal{I} \subset \mathbb{R}$ is a finite interval, which can be assumed to be $\mathcal{I} = [0, 1]$ without loss of generality. To allow for atypical observations, we will include processes $X$ for which finite second moments may not exist. Specifically, we will only assume that the process $X$ has an elliptical distribution $\mathcal{E}(\mu, \Gamma, \varphi)$, where $\mu \in L^2(\mathcal{I})$ and $\Gamma$ is a self-adjoint, positive semi-definite and Hilbert-Schmidt operator on $L^2(\mathcal{I})$. We will denote as $\gamma : L^2(\mathcal{I}) \times L^2(\mathcal{I})$ the kernel defining $\Gamma$, that is, $(\Gamma f)(s) = \int_{\mathcal{I}} \gamma(t, s) f(t) dt$. Recall that $\gamma$ is symmetric and $\int_{\mathcal{I}} \gamma^2(t, s)\, ds\, dt < \infty$, since $\Gamma$ is a Hilbert-Schmidt operator. Finally, $\{\phi_k\}_{k \geq 1}$ will denote an orthonormal basis of $L^2(\mathcal{I})$ consisting of eigenfunctions of the scatter operator $\Gamma$ ordered according to the associated non-zero eigenvalues $\lambda_1 \geq \lambda_2 \geq \ldots$.

Note that elliptically distributed random processes as defined in Section 2 accept a Karhunen-Loève representation when $\Gamma$ has finite rank or when the kernel $\gamma$ is continuous. Consider first the case where the scatter operator $\Gamma$ has finite rank (i.e. a finite number of non-zero eigenvalues). It follows that $X \sim \mu + \sum_{k=1}^{q} \xi_k \, \phi_k$, where $q = \operatorname{rank}(\Gamma)$ and $\boldsymbol{\xi} = (\xi_1, \ldots, \xi_q)^{\mathrm{T}}$ has a multivariate elliptical distribution $\mathcal{E}_q(\mathbf{0}_q, \operatorname{diag}(\lambda_1, \ldots, \lambda_q), \varphi)$ (see the proof of Proposition 3.1). When there are infinitely many positive eigenvalues, Proposition 2.1 in Boente *et al.* [7] shows that

$X \sim \mu + S\,V$, where $S \geq 0$ is a random variable independent from the zero-mean Gaussian random element $V$. The standard Karhunen-Loève expansion for Gaussian processes implies that $V = \sum_{k=1}^{\infty} \eta_k\,\phi_k(t)$ with $\eta_k \sim \mathcal{N}(0, \lambda_k)$, $k \geq 1$. The continuity of the covariance function $\gamma$ and the process $V$ implies that the convergence of the series is uniform over $\mathcal{I}$ with probability 1. Thus, defining $\xi_k = S\,\eta_k$, we obtain that $\boldsymbol{\xi} = (\xi_1, \ldots, \xi_q)^{\mathrm{T}}$ has a multivariate elliptical distribution $\mathcal{E}_q(\mathbf{0}_q, \mathrm{diag}(\lambda_1, \ldots, \lambda_q), \varphi)$ and $X \sim \mu + \sum_{k=1}^{\infty} \xi_k\,\phi_k$ with covariance operator $\Gamma$. Hence, we can write

$$X(t) = \mu(t) + \sum_{k=1}^{\infty} \xi_k\,\phi_k(t)\,, \quad t \in \mathcal{I}\,, \tag{2}$$

where the scores $\xi_k = \langle X - \mu\,, \phi_k \rangle$ are such that, for any $q \geq 1$, the random vector $\boldsymbol{\xi} = (\xi_1, \ldots, \xi_q)^{\mathrm{T}}$ has a multivariate elliptical distribution $\mathcal{E}_q(\mathbf{0}_q, \mathrm{diag}(\lambda_1, \ldots, \lambda_q), \varphi)$. When second moments exist, the scores are uncorrelated random variables.

The following Proposition provides the main motivation for our approach. It shows that, similarly to what holds for Gaussian processes, the vector obtained by evaluating an elliptically distributed random process on a fixed finite set of $k$ points is an elliptical random vector on $\mathbb{R}^k$. Furthermore, it also shows that the conditional distribution of the scores $\xi_j$ in (2) given a set of $k$ observations of the process is elliptical. This result suggests a natural estimator for the $\xi_j$'s which can be used to reconstruct the full trajectories in the sample. The proof can be found in Section 7.

**Proposition 3.1.** *Let $X \sim \mathcal{E}\,(\mu, \Gamma, \varphi)$ be a random element on $L^2(\mathcal{I})$, with $\mathcal{I} \subset \mathbb{R}$, and assume that the kernel $\gamma$ associated with $\Gamma$ is continuous. Let $\lambda_1 \geq \lambda_2 \geq \ldots$ be the non-null eigenvalues of $\Gamma$ and as $\phi_k$ the eigenfunction of $\Gamma$ associated with $\lambda_k$ chosen so that the set $\{\phi_k, k \in \mathbb{N}\}$ is an orthonormal set in $L^2(\mathcal{I})$. Then,*

*a) For any fixed $m$ and $t_1$, $t_2$, …, $t_m$ in $\mathcal{I}$, the random vector $(X(t_1), \ldots, X(t_m))^{\mathrm{T}}$ has an elliptical distribution in $\mathbb{R}^m$ with location $\boldsymbol{\mu}_m = (\mu(t_1), \ldots, \mu(t_m))^{\mathrm{T}}$ and scatter matrix $\boldsymbol{\Sigma}$ with elements $\Sigma_{(\ell,j)} = \gamma(t_\ell, t_j)$, $1 \leq \ell, j \leq m$.*

*b) For any $s_0 \neq t_0 \in \mathcal{I}$ we have that $X(t_0) \,\big|\, X(s_0) \;\sim\; \mathcal{E}_1\left(\mu_{t_0|s_0},\, \sigma_{t_0|s_0}, \varphi^{\star}_{s_0}\right)$, where the conditional location is given by*

$$\mu_{t_0|s_0} \;=\; \mu(t_0) + \frac{\gamma(t_0, s_0)}{\gamma(s_0, s_0)}\;(X(s_0) - \mu(s_0))\;. \tag{3}$$

*c) For any fixed $m$ and $t_1$, $t_2$, …, $t_m$ in $\mathcal{I}$, let $\mathbf{X}_m = (X(t_1), \ldots, X(t_m))^{\mathrm{T}}$. We have that $\xi_k \,\big|\, \mathbf{X}_m \sim \mathcal{E}_1\left(\mu_k,\, \sigma_k, \varphi^{\star}_{\mathbf{X}_m}\right)$ where*

$$\mu_k = \lambda_k\;\boldsymbol{\phi}_k^{\mathrm{T}} \boldsymbol{\Sigma}_{\mathbf{X}_m}^{-1}\,(\mathbf{X}_m - \boldsymbol{\mu}_m)\;, \tag{4}$$

*with* $\boldsymbol{\phi}_k = (\phi_k(t_1), \ldots, \phi_k(t_m))^{\mathrm{T}}$, $\boldsymbol{\mu}_m = (\mu(t_1), \ldots, \mu(t_m))^{\mathrm{T}}$ *and the* $(\ell, j)$*-th element of* $\boldsymbol{\Sigma}_{\mathbf{X}_m}$ *equals* $\gamma(t_\ell\,, t_j)$.

## 3.2 Method

In what follows we will use $\{X_i : 1 \leq i \leq N\}$ to denote independent realizations of the stochastic process $X$. We assume that each trajectory $X_i$ is observed at independent random "times" $t_{ij}$, $1 \leq j \leq n_i$, where the $n_i$'s, $1 \leq i \leq N$, are usually assumed to be random variables, independent from all others. Then, our model is:

$$X_{ij} \;=\; X_i(t_{ij}) \;=\; \mu(t_{ij}) + \sum_{k=1}^{\infty} \xi_{ik}\phi_k(t_{ij})\,, \quad j = 1, \ldots, n_i, \quad i = 1, \ldots, N\,. \tag{5}$$

The procedure has three steps: (1) estimating the center function $\mu$; (2) estimating the diagonal elements of the scatter function $\Gamma$, and (3) estimating the off-diagonal entries of $\Gamma$.

### 3.2.1 Step 1

We start by estimating the center function $\mu$ using a robust local $M$-estimator. For example, one can consider the local $M-$smoothers proposed in Boente and Fraiman [4], Härdle and Tsybakov [28], Härdle [27] and Oh *et al.* [44] or robust local linear smoothers as defined in Welsh [54]. Here we use the latter option.

Consider a $\rho$-function $\rho_1$ as defined in Maronna *et al.* [42]. That is, $\rho_1$ is even, nondecreasing as a function of $|x|$, $\rho_1(0) = 0$, and increasing for $x > 0$ when $\rho_1(x) < \sup_t \rho_1(t)$. For each $t_0 \in \mathcal{I}$, let

$$\left(\widehat{\beta}_0(t_0), \widehat{\beta}_1(t_0)\right)^{\mathrm{T}} \;=\; \underset{\beta_0,\beta_1}{\operatorname{argmin}} \sum_{i=1}^{N}\sum_{j=1}^{n_i} w_{ij}(t_0)\,\rho_1\left(\frac{X_{ij} - \beta_0 - \beta_1(t_0 - t_{ij})}{\widehat{\sigma}(t_0)}\right), \tag{6}$$

where $\widehat{\sigma}(t)$ is a preliminary robust consistent estimator of scale and the weights $w_{ij}(t_0)$ are given by

$$w_{ij}(t_0) \;=\; \mathcal{K}\left(\frac{t_{ij} - t_0}{h}\right)\left\{\sum_{k=1}^{N}\sum_{\ell=1}^{n_k}\mathcal{K}\left(\frac{t_{k\ell} - t_0}{h}\right)\right\}^{-1}, \tag{7}$$

where $h = h_n$ is a bandwidth parameter and $\mathcal{K} : \mathbb{R} \to \mathbb{R}$ is a kernel function, i.e. continuous, non-negative, and integrable. Then, the estimate for $\mu(t_0)$ is

$$\widehat{\mu}(t_0) \;=\; \widehat{\beta}_0(t_0)\,.$$

The preliminary scale estimator $\widehat{\sigma}(t_0)$ in (6) can, for example, be a "local MAD", that is: the MAD of the observations in a neighborhood of $t_0$. Formally:

$$\widehat{\sigma}(t_0) \;=\; \kappa^{-1} \underset{|t_{ij}-t_0|\leq h}{\text{median}} \left| X_{ij} - \underset{|t_{ij}-t_0|\leq h}{\text{median}} (X_{ij}) \right| ,$$

where $\kappa \in \mathbb{R}$ is a constant ensuring Fisher-consistency at a given distribution. If we consider a gaussian distribution as the central model, then $\kappa = \Phi^{-1}(3/4)$, where $\Phi$ is the cumulative distribution function of the standard normal.

### 3.2.2 Step 2

To estimate the diagonal elements $\gamma(t_0, t_0)$ of the scatter function we use a robust $M-$scale estimator of the residuals. Although in principle one can use any robust scale estimator, we expect smooth functionals (like M-scales) to provide more stable estimators. More precisely, let $\rho_2 : \mathbb{R} \to \mathbb{R}$ be a bounded $\rho$-function, such that $\sup_t \rho_2(t) = 1$, and let $b \in (0, 1)$ be a fixed constant which defines the robustness of the scale estimator (Maronna *et al.* [42]). Then $\widehat{\gamma}(t_0, t_0)$ satisfies

$$\sum_{i=1}^{N} \sum_{j=1}^{n_i} w_{ij}(t_0)\, \rho_2 \left( \frac{X_{ij} - \widehat{\mu}(t_{ij})}{\widehat{\gamma}(t_0, t_0)} \right) \;=\; b\,, \tag{8}$$

where the weights $w_{ij}(t_0)$ are as in (7). We choose $\rho_2$ so that $E(\rho_2(Z)) = b = 1/2$, where $Z \sim \mathcal{N}(0, 1)$ to ensure that in the case of i.i.d. observations with Gaussian errors, the resulting scale estimator is consistent and has maximum breakdown point.

### 3.2.3 Step 3

To estimate the off-diagonal elements $\gamma(t_0, s_0)$, $s_0 \neq t_0$, we take advantage of Proposition 3.1, which shows that the conditional mean of $X(t_0)$ given $X(s_0)$ is a linear function of the conditioning value, and furthermore, that the slope is proportional to $\gamma(t_0, s_0)$. This suggests that we can use local regression methods to estimate $\gamma(t_0, s_0)$. Specifically, we first estimate the slope $\beta(t_0, s_0)$ in (3) with a local regression estimator and then use that $\gamma(t_0, s_0) = \beta(t_0, s_0)\, \gamma(s_0, s_0)$, where $\gamma(s_0, s_0)$ can be estimated as in (8). More precisely, let $\widetilde{X}_{ij} = X_{ij} - \widehat{\mu}(t_{ij})$ be the centred observations, and let $\widehat{\beta}(t_0, s_0)$ be the local $M$-regression estimator satisfying

$$\widehat{\beta}(t_0, s_0) = \underset{\beta \in \mathbb{R}}{\text{argmin}} \sum_{i=1}^{N} \sum_{j \neq \ell} \rho \left( \frac{\widetilde{X}_{ij} - \beta \widetilde{X}_{i\ell}}{\widehat{s}(t_0, s_0)} \right) \mathcal{K} \left( \frac{t_{ij} - t_0}{h} \right) \mathcal{K} \left( \frac{t_{i\ell} - s_0}{h} \right) , \tag{9}$$

where $\widehat{s}(t_0, s_0)$ is a preliminary robust scale estimator and $\rho$ is a bounded $\rho$-function. To compute $\widehat{s}(t_0, s_0)$ we use a local MAD of the residuals from an initial robust estimator. Specifically, let $Z_{ij\ell} = \widetilde{X}_{ij}/\widetilde{X}_{i\ell}$, and noting that the model does not include an intercept, let $\widetilde{\beta}(t_0, s_0)$ be the local median of the slopes: $\widetilde{\beta}(t_0, s_0) = \text{median}_{|t_{ij}-t_0|\leq h\,,|t_{i\ell}-s_0|\leq h}\, Z_{ij\ell}$. Construct residuals $r_i(t_0, s_0) = \widetilde{X}_{ij} - \widetilde{\beta}(t_0, s_0)\, \widetilde{X}_{i\ell}$ and let $\widehat{s}(t_0, s_0)$ be the corresponding local MAD:

$$\widehat{s}(t_0, s_0) = \underset{|t_{ij}-t_0|\leq h\,,|t_{i\ell}-s_0|\leq h}{\text{median}} \left| r_i(t_0, s_0) - m(t_0, s_0) \right|,$$

with $m(t_0, s_0) = \text{median}_{|t_{ij}-t_0|\leq h\,,|t_{i\ell}-s_0|\leq h}\, r_i(t_0, s_0)$.

With $\widehat{\beta}_0(t_0, s_0)$ computed in (9) and $\widehat{\gamma}(s_0, s_0)$ from Step 2, we define

$$\widetilde{\gamma}(t_0, s_0) = \widehat{\beta}_0(t_0, s_0)\, \widehat{\gamma}(s_0, s_0)\,.$$

To ensure that the estimated function $\widehat{\gamma}$ is symmetric and smooth, we also compute $\widehat{\beta}_0(s_0, t_0)$ and use a two-dimensional smoother (e.g. a bivariate $B$-spline as described in Section 4) on each of them, resulting in $\widetilde{\widetilde{\gamma}}(s_0, t_0)$ and $\widetilde{\widetilde{\gamma}}(t_0, s_0)$. Finally, the estimated scatter function is:

$$\widehat{\gamma}(t_0, s_0) \;=\; \widehat{\gamma}(s_0, t_0) \;=\; \Big(\widetilde{\widetilde{\gamma}}(t_0, s_0) + \widetilde{\widetilde{\gamma}}(s_0, t_0)\Big) \Big/ 2\,.$$

Note that even though $\widehat{\gamma}(t, s)$ defines a symmetric kernel, it may not be semi-positive definite. If necessary, after computing its eigenvalues $\widehat{\lambda}_1 \geq \widehat{\lambda}_2 \geq \ldots$, and corresponding eigenfunctions $\widehat{\phi}_1, \widehat{\phi}_2, \ldots$, we set $\widehat{\gamma}$ as $\widehat{\gamma}(t, s) = \sum_{j:\widehat{\lambda}_j \geq 0} \widehat{\lambda}_j \widehat{\phi}_j(t)\; \widehat{\phi}_j(s)$.

### 3.2.4 Reconstructing trajectories

Once we have estimated the eigenfunctions and eigenvalues of the scatter function, Proposition 3.1(c) suggests a natural way to reconstruct the trajectories. Let $\xi_{i,k} = \langle X_i - \mu, \phi_k \rangle$ the $k$-th score of the $i$-th observation. Recall that the conditional distribution of $\xi_{i,k}$ given $\mathbf{X}_i = (X_i(t_{i1}), \ldots X_i(t_{in_i}))^{\mathrm{T}}$ is elliptical with location parameter

$$\lambda_k\, \phi_{ik}^{\mathrm{T}}\, \mathbf{\Sigma}_i^{-1}\, (\mathbf{X}_i - \boldsymbol{\mu}_i)\,, \tag{10}$$

where $\phi_{ik} = (\phi_k(t_{i1}), \ldots, \phi_k(t_{i\,n_i}))^{\mathrm{T}}$, $\boldsymbol{\mu}_i = (\mu(t_{i1}), \ldots, \mu(t_{i\,n_i}))^{\mathrm{T}}$ and $\mathbf{\Sigma}_i \in \mathbb{R}^{n_i \times n_i}$ is the matrix with $(\ell, j)-$th element equal to $\gamma(t_{i\ell}\,,\, t_{ij})$. Note that if the process has finite mean then (10) equals $\mathbb{E}\left(\xi_{i,k} \,\middle|\, \mathbf{X}_i\right)$, which is the best predictor for $\xi_{i,k}$ based on the observed trajectory.

A natural estimator for (10) consists of replacing the unknown quantities with their estimators obtained in Steps 1 - 3 above. Specifically:

$$\widehat{\xi}_{i,k} \;=\; \widehat{\lambda}_k\, \widehat{\boldsymbol{\phi}}_{ik}^{\mathrm{T}}\, (\widehat{\mathbf{\Sigma}}_i + \delta \mathbf{I}_{n_i})^{-1}\, (\mathbf{X}_i - \widehat{\boldsymbol{\mu}}_i)\,, \tag{11}$$

where $\widehat{\boldsymbol{\mu}}_i = (\widehat{\mu}(t_{i1}), \ldots \widehat{\mu}(t_{in_i}))^{\mathrm{T}}$, $\widehat{\boldsymbol{\phi}}_{ik} = \left(\widehat{\phi}_k(t_{i1}), \ldots \widehat{\phi}_k(t_{in_i})\right)^{\mathrm{T}}$, $\widehat{\boldsymbol{\Sigma}}_i$ is the matrix with $(j,\ell)-$th element $\widehat{\gamma}(t_{ij}, t_{i\ell})$, and $\delta > 0$ is a small regularization constant to ensure non-singularity (see Yao *et al.* [56]). Finally, for a fixed $q$, the reconstructed curves are

$$\widehat{X}_i \;=\; \sum_{k=1}^{q} \widehat{\xi}_{i,k}\, \widehat{\phi}_k\,, \qquad i = 1, \ldots, n\,.$$

### 3.3 The non-robust case

Note that using $\rho(u) = \rho_1(u) = \rho_2(u) = u^2$ in the method described above naturally yields a non-robust version of our proposal, which is different from that of Yao *et al.* [56]. Moreover, our numerical experiments (see Section 4) indicate that when the data do not contain outliers the non-robust version of our proposal compares favourably to PACE (Yao *et al.* [56]).

## 4 Monte Carlo study

In this section we report the results of a Monte Carlo study carried out to investigate the finite-sample performance and robustness of the proposed robust FPCA estimator. Our experiments compared the robust and non-robust versions of our proposal and PACE, the approach in Yao *et al.* [56]. We report results for random processes with two covariance functions and different atypical observations. In each case we generated 500 samples of size $N = 100$, and focused on the behaviour of the estimated eigenfunctions, eigenvalues, predicted scores, and accuracy of the scatter function estimator for both clean and contaminated samples.

### 4.1 Simulation settings

For clean samples, the data sets are generated from the following model

$$X_i \;=\; \mu \,+\, \sum_{j=1}^{q} \sqrt{\lambda}_j\, Z_{ij}\, \phi_j\,, \qquad i = 1, \ldots N\,, \tag{12}$$

with $Z_{ij}$ i.i.d. $Z_{ij} \sim \mathcal{N}(0,1)$ and $\lambda_1 \geq \lambda_2 \geq \cdots \lambda_q > 0$. We considered two models for the location function $\mu$ and the principal directions $\phi_j$:

- **Model 1:** $\mathcal{I} = (0, 10)$, $\mu(t) = t \,+\, \sin(t)$ $q = 2$, $\lambda_1 = 4$, $\lambda_2 = 1$ and $\phi_j$ two

elements of the Fourier basis:

$$\phi_1(t) = -\frac{\cos(t\,\pi/10)}{\sqrt{5}}\,, \qquad \phi_2(t) = \frac{\sin(t\,\pi/10)}{\sqrt{5}}\,.$$

The design points were generated as follows. First build an equally spaced grid of 51 points $\{c_\ell\}_{\ell=1}^{51}$ on $[0, 10]$ with $c_1 = 0$ and $c_{51} = 10$, and define $s_\ell = c_\ell + \epsilon_\ell$, where $\epsilon_\ell$ are i.i.d. with $\epsilon_\ell \sim N(0, 0.1)$ (set $s_\ell = 0$ if $s_\ell < 0$, and $s_\ell = 10$ when $s_\ell > 10$). Each curve was sampled at a random number of points $n_i$, chosen from a discrete uniform distribution on $\{2, 3, 4\}$, and the locations $t_{ij}$ were randomly chosen from $\{s_\ell\}_{\ell=2}^{50}$ without replacement. This is the same setting as in Yao *et al.* [56].

- **Model 2:** In this case, $\mathcal{I} = (0, 1)$, $\mu(t) = 10\,\sin(2\,t\,\pi)\,\exp(-3\,t)$, $q = 4$, $\lambda_1 = 0.83$, $\lambda_2 = 0.08$, $\lambda_3 = 0.029$ and $\lambda_4 = 0.015$, and the eigenfunctions $\phi_j$ are the first $q$ eigenfunctions of the "Mattern" covariance function:

$$\gamma(s,t) \;=\; C\left(\frac{\sqrt{2\nu}\,|s-t|}{\rho}\right)\,, \quad C(u) = \frac{\sigma^2\,2^{1-\nu}}{\Gamma(\nu)}\,u^\nu K_\nu\,(u)\;,$$

where $\Gamma(\cdot)$ is the Gamma function and $K_\nu$ is the modified Bessel function of the second kind. We set $\rho = 3$, $\sigma = 1$ and $\nu = 1/3$. The eigenvalues above were chosen to have very similar ratios $\lambda_j/\lambda_{j+1}$, $j = 1, 2, 3$ to those of the first 4 eigenvalues of this Mattern covariance function. To obtain sparsely observed trajectories each curve was observed at a random number of times $n_i$ chosen from a discrete uniform distribution on $\{3, 4, 5\}$. The observed times $t_{ij}$ satisfy $t_{ij} \sim \mathcal{U}(\mathcal{I})$, i.i.d., $j = 1, \ldots, n_i; i = 1, \ldots, N$.

These models have different characteristics that may affect the performance of the FPCA estimators on finite samples. For example, while the ratio between the first and second eigenvalues is 4 for Model 1, it is larger than 10 for Model 2. This means that in the second model a single principal direction already explains a larger proportion (87%) of the total variation. In addition, although the first two principal directions are similar in both models (with the order reversed), the third and fourth eigenfunctions of Model 2 will tend to produce less smooth trajectories, and a slightly more complex covariance function.

Figure 1 illustrates typical samples obtained under each Model. We highlighted 3 randomly chosen trajectories in each sample. The filled circles correspond to the observations.

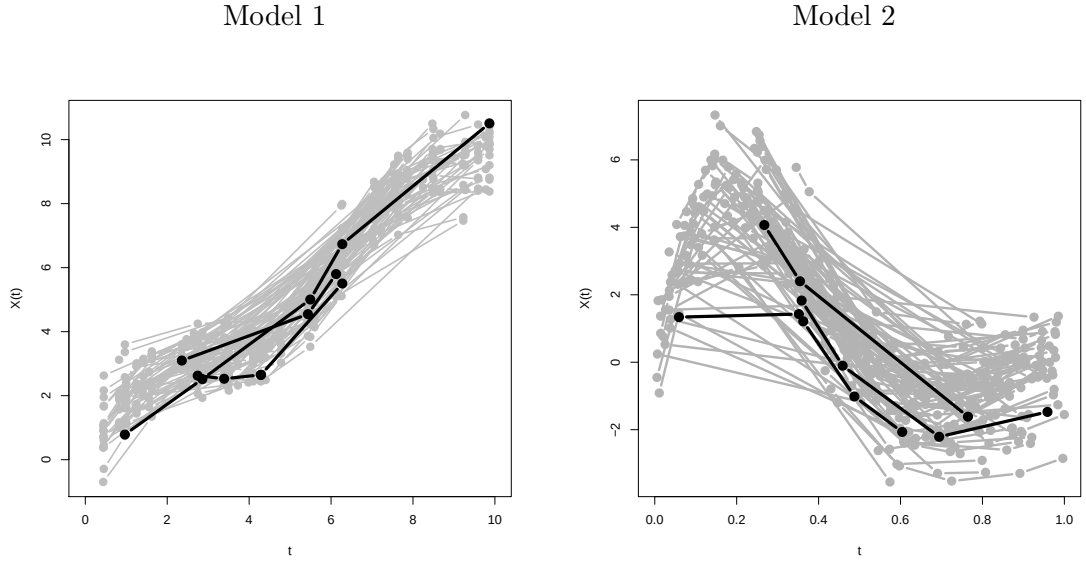



Figure 1: One typical sample from each Model, with 3 randomly chosen trajectories highlighted. Filled circles correspond to available observations.

### 4.2 Outliers

Atypical observations were introduced to alter the order among the principal directions so that the estimated eigenfunctions and eigenvalues might be affected. Outliers were introduced using a Bernoulli random variable $B_i \sim \mathcal{B}(1, \epsilon)$, $i = 1, \ldots, N$, with $\epsilon = 0.05$ or $0.10$, which correspond to 5% and 10% of outliers, respectively. When $B_i = 0$ the trajectory $X_i$ is generated as in (12). When $B_i = 1$ the curve is contaminated as follows:

- **Model 1**: The score $Z_{i,2}$ for the second direction is sampled from $Z_{i,2} \sim \mathcal{N}(12, 1)$;
- **Model 2**: The scores for the second and third direction are sampled from the following bivariate distribution:

$$\begin{pmatrix} Z_{i,2} \\ Z_{i,3} \end{pmatrix} \sim \mathcal{N}(\boldsymbol{\mu}_c, \boldsymbol{\Sigma}_c) \quad \text{with} \quad \boldsymbol{\mu}_c = \begin{pmatrix} 20 \\ 25 \end{pmatrix} \quad \text{and} \quad \boldsymbol{\Sigma}_c = \begin{pmatrix} 1/16 & 0 \\ 0 & 1/16 \end{pmatrix}.$$

Figure 2 shows how the introduced contaminations modify the pattern of the clean data when $\epsilon = 0.10$. Black solid lines correspond to two randomly chosen

uncontaminated observations, and dashed red lines indicate 3 randomly selected outlying trajectories.

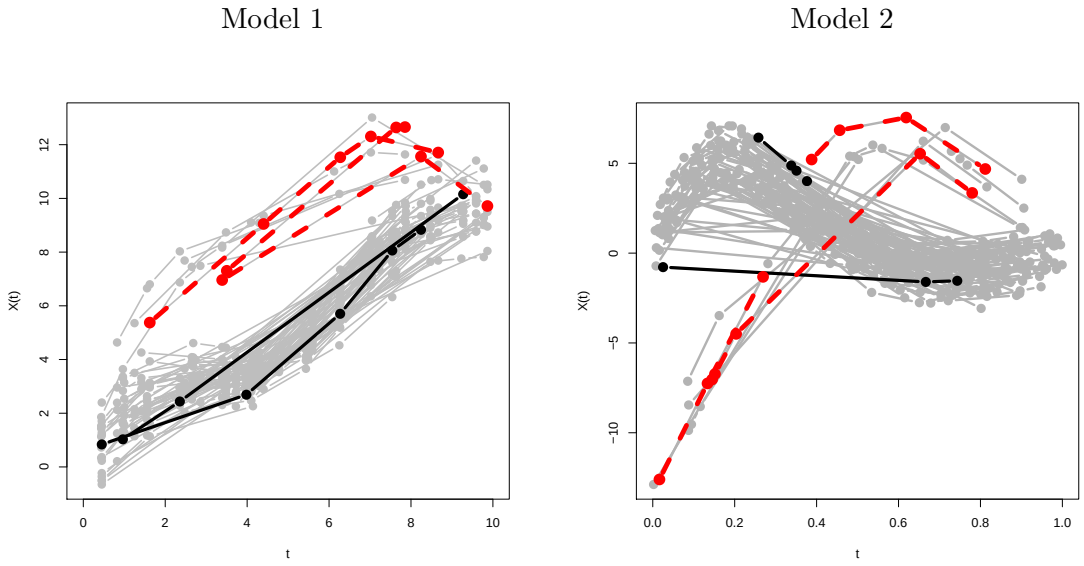



Figure 2: Contaminated sample from Models 1 to 3 with $\epsilon = 0.10$. The filled points correspond to the observed trajectories. Black solid lines correspond to two randomly chosen uncontaminated observations, and dashed red lines indicate 3 randomly selected outlying trajectories (color figures are available on the web version of this article).

### 4.3 The estimators

We considered three estimators: two of them are based on non-resistant procedures and the third one is our proposal in Section 3. Of the two non-robust methods, one is PACE (Yao *et al.* [56]), and the other is the non-robust version of our method as in Section 3.3. All computations were done using `R` (R Core Team [46]). The PACE estimator was computed using the package `fdapace` (Chen *et al.* [12]). Our estimators were computed using `R` code in the package `sparseFPCA` publicly available at `https://github.com/msalibian/sparseFPCA`.

The tuning parameters for the robust FPCA estimator were chosen as follows. To estimate $\mu(t)$ we use a Huber function $\rho$ with constant 1.345. In Steps 2 and 3 we use $\rho$-functions in Tukey's biweight family. To estimate the diagonal elements of the scatter function $\gamma(t,t)$ the tuning constants were $c = 1.54764$ and $b = 1/2$. In Step 3, to obtain a more efficient estimator for $\beta(t,s)$, we used a larger tuning constant.

More specifically, we selected $c = 3.44369$, which in linear regression models leads to estimators with breakdown point 1/2 and asymptotic efficiency 0.85.

The kernel function in (7) and (9) was an Epanechnikov kernel, $\mathcal{K}(u) = 0.75\,(1 - u^2)\mathbb{I}_{[-1,1]}(u)$. The two–dimensional smoother used in Step 3 was a thin plate regression spline, as described in Section 5.5.1 of Wood [55], which does not require selecting knot locations. The bandwidth parameters were selected using a robust 5-fold cross-validation (holding 20% of the curves for each fold). The cross-validation criterion for the robust estimator was based on a 50% breakdown point $M$-scale of the residuals with respect to the fits in equations (6) and (9), while for the other two approaches we used the mean squared prediction error.

We chose the number $K$ of principal directions to estimate with the goal of explaining at least 90% of the total variability. This corresponds to $K = 2$ for both Models above.

### 4.4 Simulation results

To compare the different approaches we look at the corresponding scatter operators $\widehat{\Gamma}$, their associated eigenvalues and eigenfunctions and the predicted scores. We report summaries of their performance computed over 500 samples of $N = 100$ trajectories each, generated under each Model using clean and contaminated data.

To quantify the discrepancy between the estimated $\widehat{\Gamma}$ and the true $\Gamma$ scatter operators we use the following approximation to the norm of their difference. We compute the operators over a fixed grid of 50 equidistant points in $\mathcal{I}$, and calculate the squared Frobenius norm of the difference matrix. This is a discrete version of the corresponding operator norm for Hilbert-Schmidt operators $\Upsilon$ given by $\|\Upsilon\|_{\mathcal{F}}^2 = \operatorname{trace}[\Upsilon^*\Upsilon] = \sum_{j=1}^{\infty} \|\Upsilon u_j\|^2$, with $\{u_j : j \geq 1\}$ any orthonormal basis of $L^2(\mathcal{I})$.

To compare the different eigenvalue estimators we consider two loss measures:

$$\frac{1}{500}\sum_{\ell=1}^{500}\left\{\log\left(\frac{\widehat{\lambda}_{\ell,k}}{\lambda_k}\right)\right\}^2, \qquad \text{and} \qquad \frac{1}{500}\sum_{\ell=1}^{500}\left\{\left(\frac{\widehat{\lambda}_{\ell,k}}{\lambda_k} - 1\right)\right\}^2,$$

where $\widehat{\lambda}_{\ell,k}$ is the estimated $k$-th eigenvalue obtained with the $\ell$-th sample.

The accuracy of the eigenfunction estimators was measured using the cosine of the angle between the estimated and true eigenfunctions. Values close to 1 correspond to a small angle and thus to a good estimated eigenfunction, whereas values close to zero indicate estimated eigenfunctions that are close to being orthogonal to

the true ones. We report

$$\frac{1}{500}\sum_{\ell=1}^{500}\cos(|\langle\widehat{\phi}_{\ell,k},\phi_k\rangle|)\,,$$

where $\widehat{\phi}_{\ell,k}$ and $\phi_k$ are the estimated $k$-th eigenfunction computed with the $\ell$-th sample, and the true $k$-th eigenfunction, respectively.

Finally, to measure the discrepancy between the true and predicted scores, for each $k$, we calculate the average of the scores distances over the observations in each sample:

$$\mathrm{MSE}_\ell(\xi_k) = (1/N)\sum_{i=1}^{N}\left(\widehat{\xi}_{i,k}^{(\ell)} - \xi_{i,k}^{(\ell)}\right)^2\,, \quad \ell = 1,\ldots,500\,,$$

where $\xi_{i,k}^{(\ell)}$ and $\widehat{\xi}_{i,k}^{(\ell)}$ denote the true and the estimated $k$-th score for the $i$-th trajectory of the $\ell$-th sample, $1 \le k \le K$, respectively. For each $k = 1, 2$, we report the mean and median of $\mathrm{MSE}_\ell(\xi_k)$ over the $\ell = 1,\ldots,500$ replications.

Note that, for a fixed $k$, the predicted scores $\widehat{\xi}_{i,k}$ defined in (11) may be multiplied by -1 when the $k-$th estimated eigenfunction is multiplied by -1, without changing the predicted trajectory. For that reason, in order to ensure that both the true and predicted scores have the same *orientation*, for each replication $\ell$ and each $k$, we compute the Spearman correlation $s_k^{(\ell)}$, between $\widehat{\xi}_{i,k}^{(\ell)}$ and $\xi_{i,k}^{(\ell)}$, $1 \le i \le N$. When $s_k^{(\ell)} < 0$, we redefine the scores $\widehat{\xi}_{i,k}^{(\ell)}$, $1 \le i \le N$, multiplying by -1 those originally obtained.

In what follows the method proposed by Yao *et al.* [56] will be denoted PACE, our robust method method will be labeled ROB, and our non-robust variant (Section 3.3) LS. Results for experiments without outliers will be indicated with the label $C_0$, while those corresponding to the contamination schemes described in Section 4.1 will be indicated with $C_{0.05}$ and $C_{0.10}$ when $\epsilon = 0.05$ and 0.10, respectively.

Taking into account that the squared operator norm and the mean scores distances $\mathrm{MSE}_\ell(\xi_k)$ are non-negative and expected to have a skewed distribution, we use skewed-adjusted boxplots (Hubert and Vandervieren [33]) to display our results. These can be found in Figures 3, 4 and 6.

As expected, when no outliers are present all procedures are comparable, with the robust procedure performing slightly worse than the non-robust methods when estimating the scatter operator, in particular under Model 1 (Table 1). Note that for both Models the non-robust version of our approach (LS) shows the best performance. Figures 3 and 4 confirm this observation. The stability and advantage of ROB over PACE and LS when outliers are present in the data can be seen in

Table 1, and Figures 3 and 4.

Table 2 contains the average of the cosine of the angles between the estimated and true eigenfunctions. Here again LS has the best performance for clean data, although the difference between the three estimators is small. For contaminated data sets (even with only 5% of outliers) the estimated eigenfunctions obtained with PACE and LS are heavily affected by the atypical observations, while the robust estimator remains stable.

Tables 3 and 4 show the results for the eigenvalue estimators. Note that under Model 1, even without contamination, all estimators for $\lambda_1$ are biased (this can be observed in Figure 5). When the samples are contaminated the robust eigenvalue estimators perform better than the non-robust ones. The results for Model 2 are as one would expect: very little difference when no outliers are present in the data, and a noticeable advantage of the robust estimator in the contaminated settings.

The predicted scores of all estimators with clean samples behave very similar to each other (Tables 5 and 6). Note that the larger values of the mean and median of $\text{MSE}(\xi_k)$, under Model 1, may be explained by the fact that $\text{VAR}(\xi_{ik}) = \lambda_k$, and the eigenvalues of Model 1 are larger than those for Model 2. When no outliers are present the LS estimator performs best.

Noting that score estimates can be highly influenced by atypical trajectories, to evaluate the fit over the uncontaminated curves, we also considered the average over replications, $M_2(\xi_k)$, of the following quantity:

$$M_{2,\ell}(\xi_k) \quad = \quad \frac{1}{\sum_{i=1}^{N}(1-B_i)} \sum_{i=1}^{N}(1-B_i)\left(\widehat{\xi}_{i,k}^{(\ell)} - \xi_{i,k}^{(\ell)}\right)^2 .$$

We expect a good procedure to fit well most of the uncontaminated data, resulting in small values of $M_{2,\ell}(\xi_k)$. Note that, for clean samples, $M_{2,\ell}(\xi_k)$ equals $\text{MSE}_\ell(\xi_k)$. Figure 7 and Table 7 show that classical procedures result in a compromise between outlying and non-outlying trajectories, leading to bad predictions for the uncontaminated data. Under the contamination settings in this study, the robust estimator has the best performance overall. The scores mean squared error of the robust approach is the smallest, sometimes by a factor larger than 6 (see Table 5). Table 7 reveals that the robust procedure also provides better fits to the non-contaminated samples. For $\epsilon = 0.05$, the values of $M_2$ for the robust method are similar to those obtained under $C_0$, while for $\epsilon = 0.10$ they increase by a factor less than 2.5. The values of $M_2$ for PACE and LS, when the data contain outliers, can be more than 10 times higher than their values under $C_0$.

| | Model 1 | | | Model 2 | | |
|---|---|---|---|---|---|---|
| | ROB | LS | PACE | ROB | LS | PACE |
| $C_0$ | 0.0256 | 0.0133 | 0.0154 | 0.0468 | 0.0230 | 0.0398 |
| $C_{0.05}$ | 0.0235 | 0.5344 | 0.4668 | 0.0887 | 3.5896 | 6.0193 |
| $C_{0.10}$ | 0.0584 | 1.7041 | 1.3851 | 0.3228 | 12.3002 | 17.5266 |

Table 1: Average of $\|\widehat{\Gamma} - \Gamma\|_{\mathcal{F}}^2$ over 500 samples.

| | | $\widehat{\phi}_1$ | | | $\widehat{\phi}_2$ | | |
|---|---|---|---|---|---|---|---|
| | | ROB | LS | PACE | ROB | LS | PACE |
| Model 1 | $C_0$ | 0.9622 | 0.9923 | 0.9872 | 0.9483 | 0.9812 | 0.9594 |
| | $C_{0.05}$ | 0.9486 | 0.2304 | 0.3015 | 0.9388 | 0.2297 | 0.3022 |
| | $C_{0.10}$ | 0.8521 | 0.0898 | 0.1189 | 0.8468 | 0.0905 | 0.1215 |
| Model 2 | $C_0$ | 0.9919 | 0.9977 | 0.9938 | 0.9198 | 0.9776 | 0.8586 |
| | $C_{0.05}$ | 0.9878 | 0.4388 | 0.3940 | 0.8821 | 0.3867 | 0.3396 |
| | $C_{0.10}$ | 0.9390 | 0.1889 | 0.1982 | 0.8165 | 0.1725 | 0.1881 |

Table 2: Average of $\cos(|\langle\widehat{\phi}_{\ell,k}, \phi_k\rangle|)$ over $\ell = 1, \ldots, 500$, for $k = 1, 2$.

| | | $k=1$ | | | $k=2$ | | |
|---|---|---|---|---|---|---|---|
| | | ROB | LS | PACE | ROB | LS | PACE |
| Model 1 | $C_0$ | 0.2652 | 0.1187 | 0.0628 | 0.0685 | 0.0931 | 0.0530 |
| | $C_{0.05}$ | 0.1228 | 0.4714 | 0.4058 | 0.2141 | 1.1298 | 1.3880 |
| | $C_{0.10}$ | 0.0786 | 1.4122 | 1.1931 | 0.6719 | 1.4483 | 1.6548 |
| Model 2 | $C_0$ | 0.0376 | 0.0259 | 0.0339 | 0.1059 | 0.1525 | 0.1772 |
| | $C_{0.05}$ | 0.0505 | 0.6590 | 1.0158 | 0.5273 | 4.3406 | 4.5832 |
| | $C_{0.10}$ | 0.0934 | 1.8684 | 2.3644 | 2.0295 | 5.2132 | 5.6738 |

Table 3: Average of $(\log(\widehat{\lambda}_{\ell,k}/\lambda_k))^2$ over $\ell = 1, \ldots, 500$, for $k = 1, 2$.

| | | $k=1$ | | | $k=2$ | | |
|---|---|---|---|---|---|---|---|
| | | ROB | LS | PACE | ROB | LS | PACE |
| Model 1 | $C_0$ | 0.1390 | 0.0760 | 0.0493 | 0.0838 | 0.0586 | 0.0569 |
| | $C_{0.05}$ | 0.0763 | 1.2663 | 1.0439 | 0.4461 | 4.1994 | 5.8317 |
| | $C_{0.10}$ | 0.0776 | 6.1153 | 4.6775 | 2.0962 | 6.2134 | 7.7069 |
| Model 2 | $C_0$ | 0.0344 | 0.0233 | 0.0283 | 0.1662 | 0.0913 | 0.2062 |
| | $C_{0.05}$ | 0.0659 | 2.6433 | 5.0494 | 1.9130 | 66.5294 | 76.7619 |
| | $C_{0.10}$ | 0.1608 | 12.0135 | 17.9939 | 17.6268 | 95.6142 | 124.1025 |

Table 4: Average of $((\widehat{\lambda}_{\ell,k}/\lambda_k) - 1)^2$ over $\ell = 1, \ldots, 500$, for $k = 1, 2$.

| | | $k=1$ | | | $k=2$ | | |
|---|---|---|---|---|---|---|---|
| | | ROB | LS | PACE | ROB | LS | PACE |
| Model 1 | $C_0$ | 0.2787 | 0.1715 | 0.3828 | 0.2746 | 0.1149 | 0.3011 |
| | $C_{0.05}$ | 0.9717 | 8.7177 | 8.3245 | 0.8070 | 9.3234 | 8.6898 |
| | $C_{0.10}$ | 3.6692 | 14.8339 | 15.1670 | 3.1779 | 16.9066 | 16.6332 |
| Model 2 | $C_0$ | 0.0461 | 0.0386 | 0.0427 | 0.0510 | 0.0401 | 0.0413 |
| | $C_{0.05}$ | 0.3319 | 1.9847 | 1.9123 | 0.4021 | 1.5955 | 1.5153 |
| | $C_{0.10}$ | 0.8653 | 4.2007 | 3.8671 | 0.8770 | 3.3106 | 3.0065 |

Table 5: Average of $\mathrm{MSE}_\ell(\xi_k)$ over $\ell = 1, \ldots, 500$, for $k = 1, 2$.

| | | $k=1$ | | | $k=2$ | | |
|---|---|---|---|---|---|---|---|
| | | ROB | LS | PACE | ROB | LS | PACE |
| Model 1 | $C_0$ | 0.1864 | 0.1560 | 0.3640 | 0.1315 | 0.1004 | 0.2823 |
| | $C_{0.05}$ | 0.3960 | 9.2000 | 8.7213 | 0.3944 | 9.6801 | 8.8836 |
| | $C_{0.10}$ | 0.8955 | 14.8595 | 15.2054 | 0.9741 | 16.6023 | 16.3510 |
| Model 2 | $C_0$ | 0.0425 | 0.0352 | 0.0397 | 0.0470 | 0.0385 | 0.0367 |
| | $C_{0.05}$ | 0.2421 | 1.9905 | 1.9149 | 0.2965 | 1.5463 | 1.4494 |
| | $C_{0.10}$ | 0.5115 | 4.3153 | 3.8731 | 0.6043 | 3.3486 | 2.9270 |

Table 6: Median of $\mathrm{MSE}_\ell(\xi_k)$ over $\ell = 1, \ldots, 500$, for $k = 1, 2$.

| | | $k=1$ | | | $k=2$ | | |
|---|---|---|---|---|---|---|---|
| | | ROB | LS | PACE | ROB | LS | PACE |
| Model 1 | $C_0$ | 0.2787 | 0.1715 | 0.3828 | 0.2746 | 0.1149 | 0.3011 |
| | $C_{0.05}$ | 0.3259 | 3.8781 | 3.6919 | 0.3866 | 3.2214 | 3.1439 |
| | $C_{0.10}$ | 0.7847 | 5.6363 | 5.6406 | 0.9642 | 3.4723 | 3.8266 |
| Model 2 | $C_0$ | 0.0461 | 0.0386 | 0.0427 | 0.0510 | 0.0401 | 0.0413 |
| | $C_{0.05}$ | 0.0578 | 0.6877 | 0.7245 | 0.0876 | 0.5497 | 0.4676 |
| | $C_{0.10}$ | 0.1226 | 1.4081 | 1.3645 | 0.1936 | 0.6895 | 0.5456 |

Table 7: Summary measure $M_2$ for the scores.

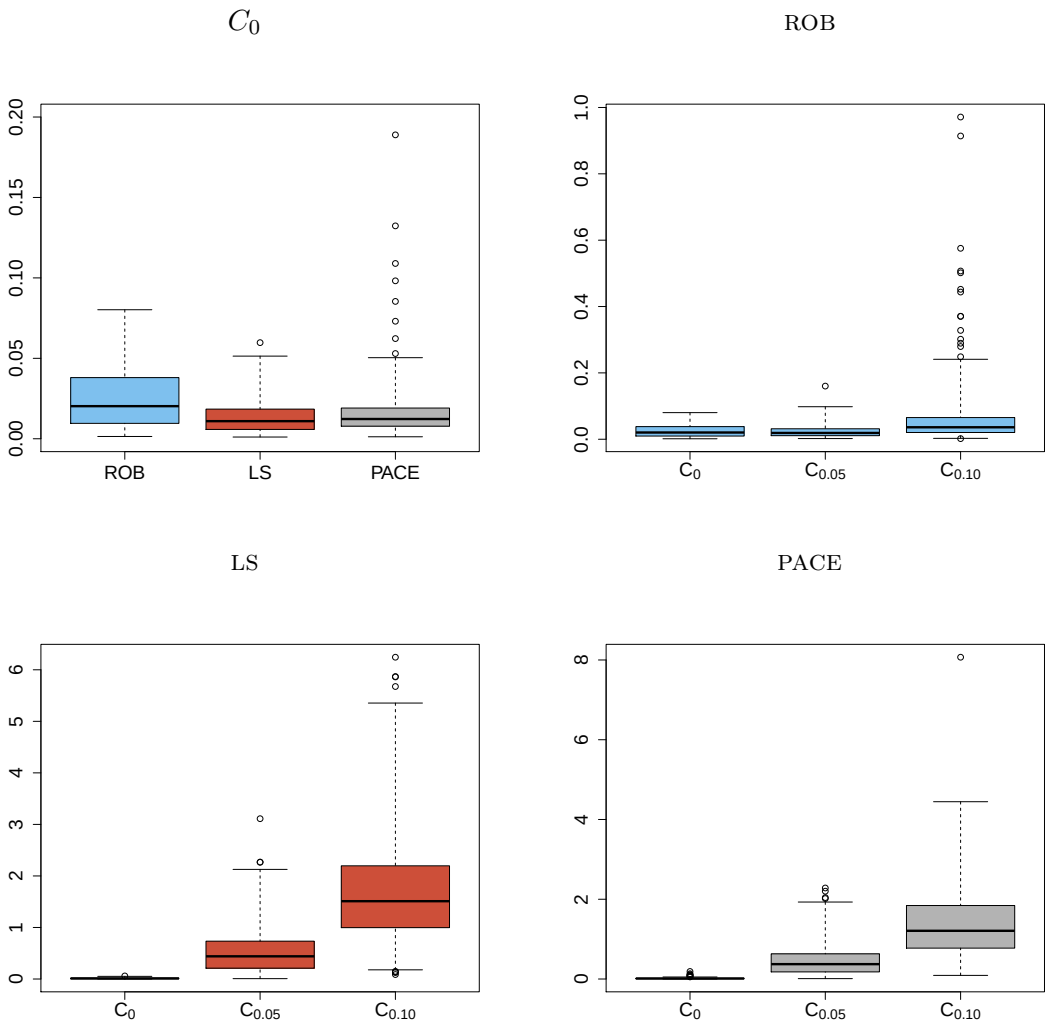



Figure 3: Adjusted boxplots of $\|\widehat{\Gamma} - \Gamma\|_{\mathcal{F}}^2$, under Model 1.

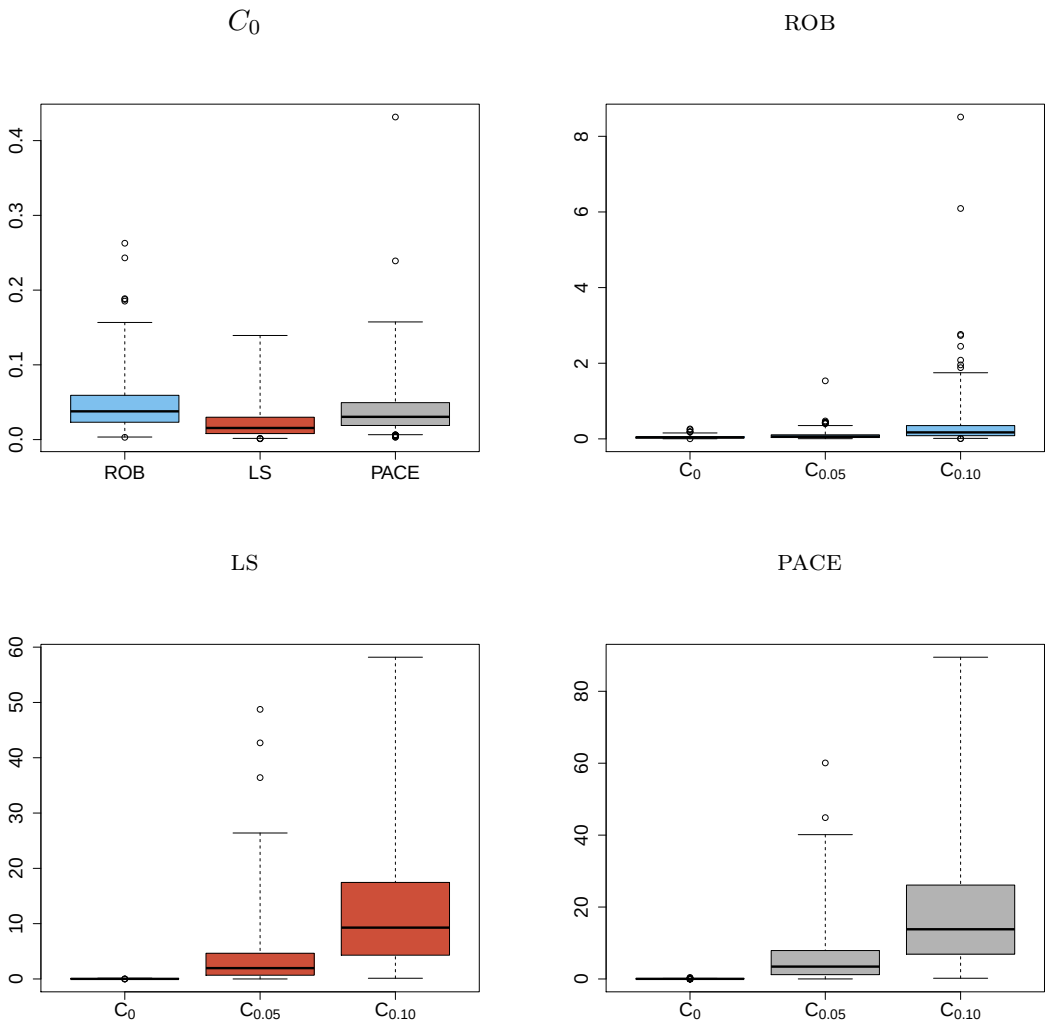



Figure 4: Adjusted boxplots of $\|\widehat{\Gamma} - \Gamma\|_{\mathcal{F}}^2$, under Model 2.

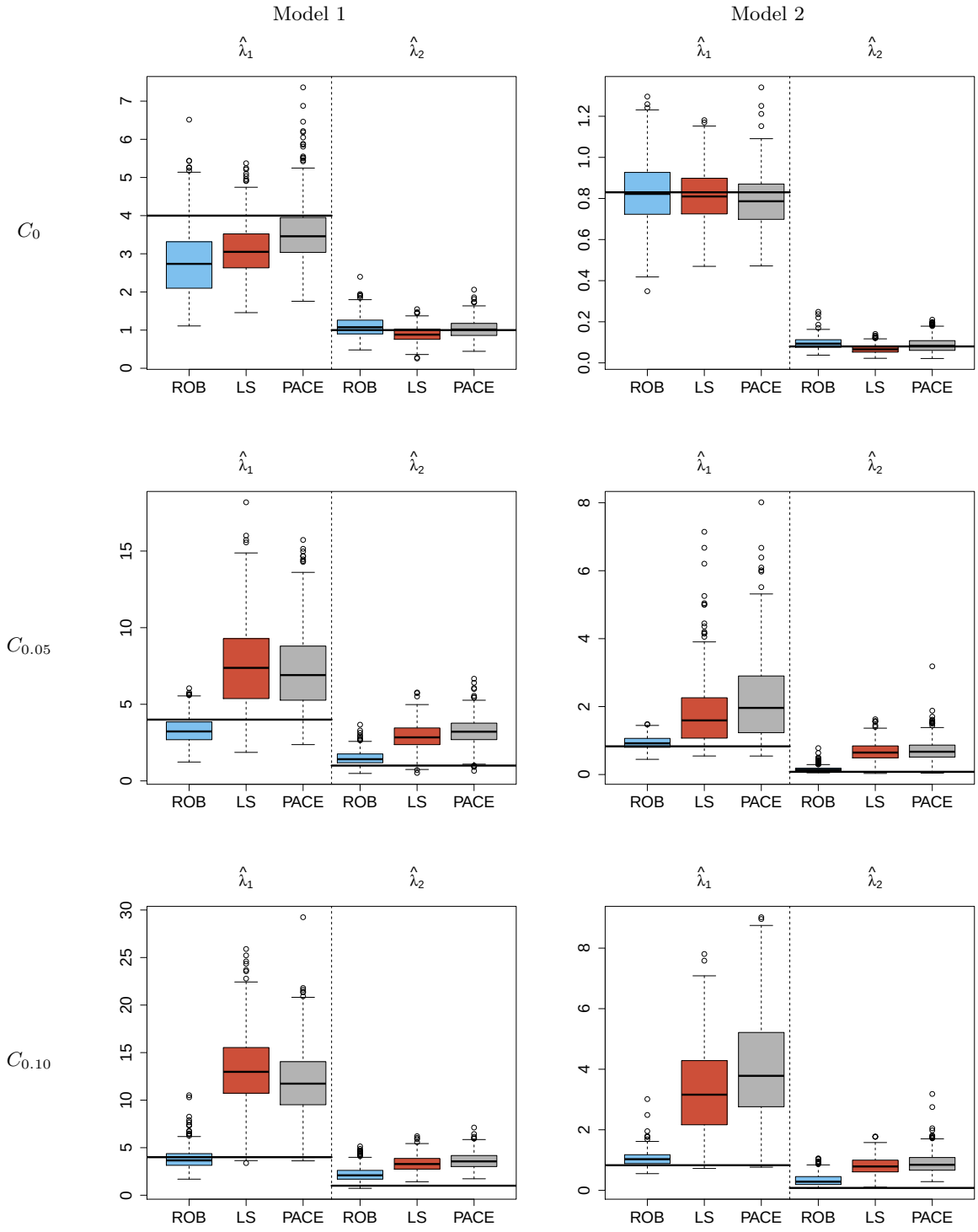



Figure 5: Boxplots of $\widehat{\lambda}_j$, for $j = 1, 2$. The horizontal lines indicate the value of the true eigenvalues $\lambda_j$.

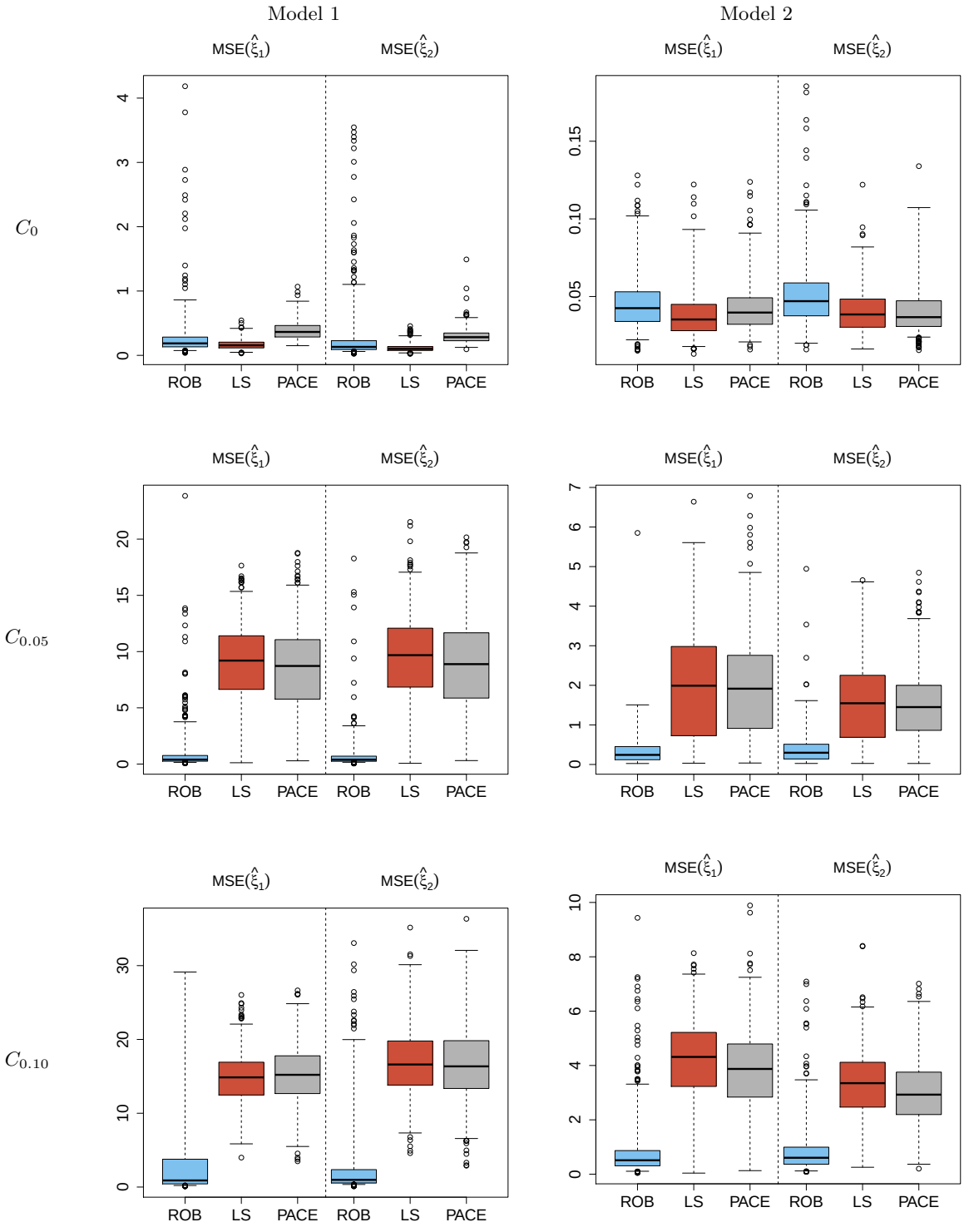



Figure 6: Adjusted boxplots of the mean scores distance $\mathrm{MSE}_\ell(\xi_k)$, $k = 1, 2$.

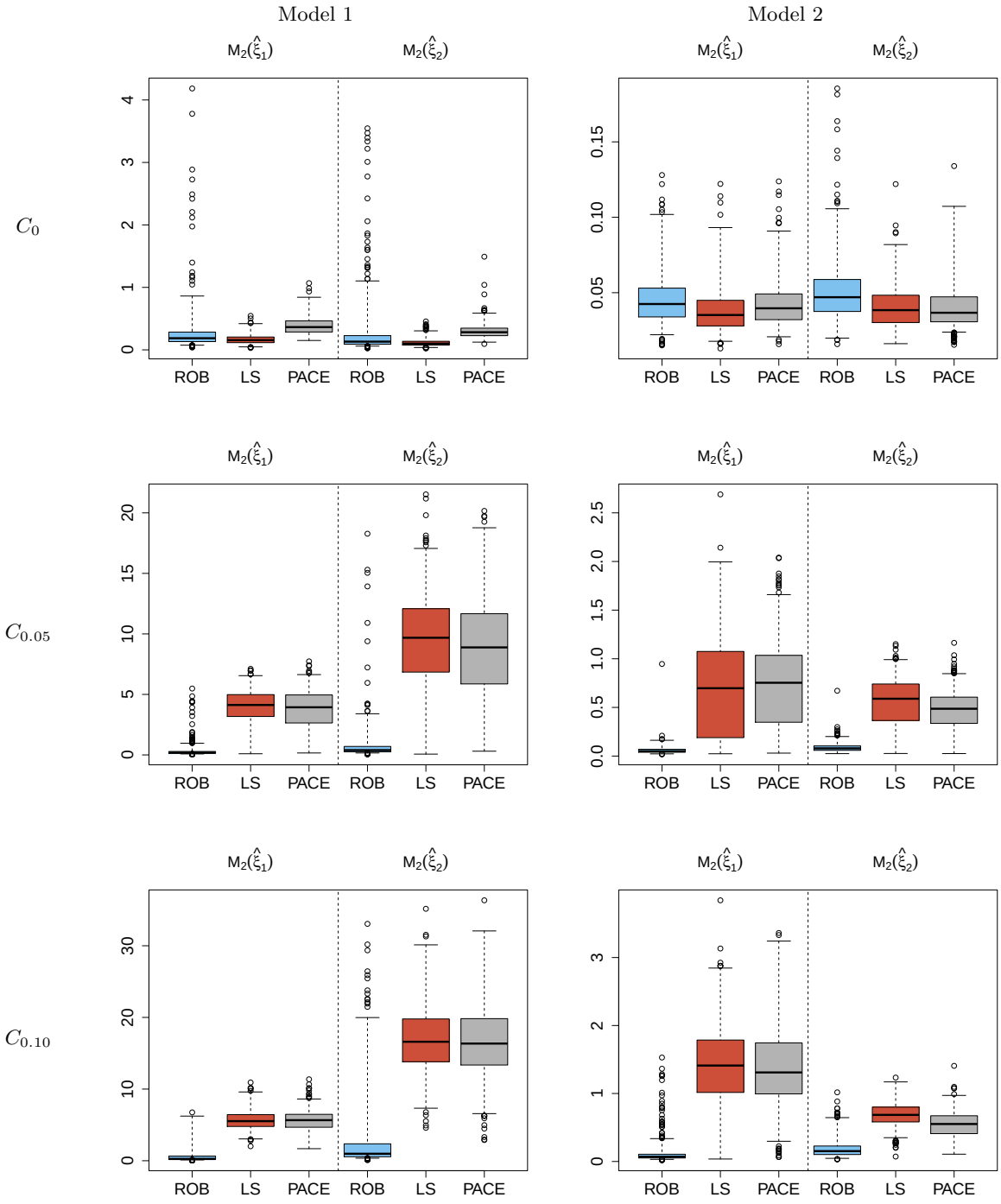



Figure 7: Adjusted boxplots of $M_{2,\ell}(\xi_k)$ for $k = 1, 2$.

# 5 A real data example

We illustrate our method on the CD4 data, which is part of the Multicentre AIDS Cohort Study (Zeger and Diggle [57]). The data consists of 2376 measurements of CD4 cell counts, taken on 369 men. The times are measured in years since seroconversion ($t = 0$). The whole data set is available from the `catdata` package for `R` (Schauberger and Tutz [49]). To ensure that there are enough observations to estimate the covariance function at every pair of times $(s, t)$, we focus on the observations with $t \geq 0$, and on individuals with more than one measurement. This results in $N = 292$ curves, with the number of observations per individual ranging between 2 and 11 (with a median of 5). The data set is shown in Figure 8, with three randomly chosen trajectories highlighted with solid black lines.

(a) Data (b) Most outlying curves

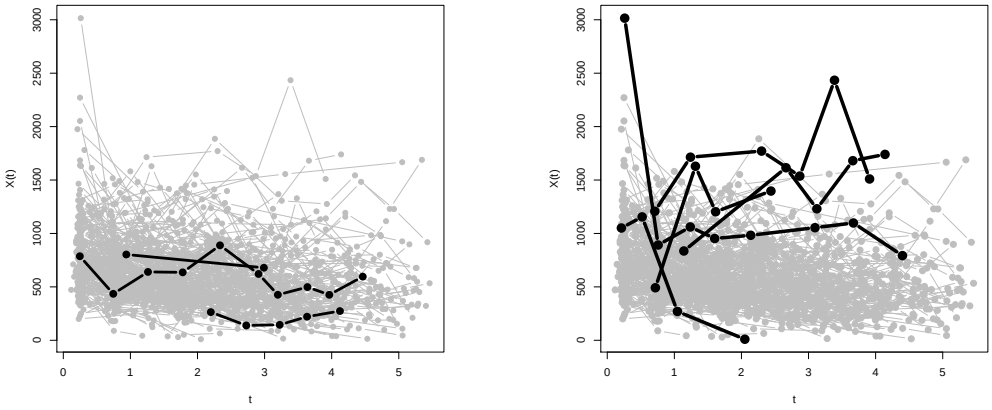



Figure 8: CD4 counts for $N = 292$ patients where $t \geq 0$. Three randomly chosen curves are highlighed with solid black lines on the left panel, while the right panel shows the five most outlying trajectories.

We compare the covariance function estimates obtained with our robust FPCA method in Section 3.2 (ROB), the corresponding non-robust variant (Section 3.3) (LS) and PACE (Yao *et al.* [56]). The tuning parameters and bandwidths for ROB and LS were chosen as in the simulation study (Section 4.3) using 10-fold cross-validation, while the smoothing parameters for PACE were set as described in Wang *et. al* [53].

The first two principal components estimated with ROB and LS account for over

99% of the total variability, while for PACE they reach over 94%. Figures 9 and 10 show the estimated covariance functions and eigenfunctions, respectively.

(a) ROB (b) LS (c) PACE

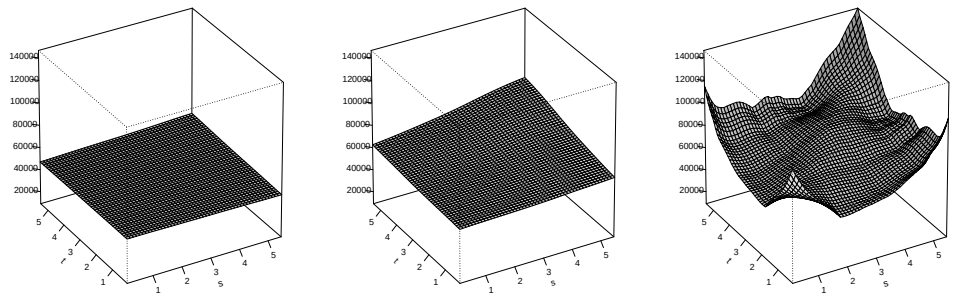


Figure 9: Estimated covariance functions for the three estimators (ROB, LS and PACE).

Although the estimated first principal directions are similar for the three methods, the PACE estimate for the second eigenfunction is notably different. To explore the possibility that this difference is due to the effect of a few potentially atypical observations, we identify outliers using the scores $(\hat{\xi}_{i1}, \hat{\xi}_{i2})$, $i = 1, \ldots, 292$, of the curves based on the first 2 robustly estimated eigenfunctions. To decide which score vectors may be outliers, we compute their robust Mahalanobis distance $D_i$ using an $MM-$location and scatter estimator. We flag as outliers those vectors $(\hat{\xi}_{i1}, \hat{\xi}_{i2})$ with $D_i^2$ larger than the 99.5% quantile of a $\chi_2^2$ distribution. This resulted in 18 trajectories being identified as potentially atypical. The five most outlying ones are shown in the right panel of Figure 8. Note that these curves appear to either decrease too rapidly (with respect to the rest), or to remain at high values over time. The other outlying curves also show one of these these two main patterns. More details about this analysis, including documented `R` code reproducing these analyses is publicly available on-line at `https://github.com/msalibian/sparseFPCA`. We now re-compute the non-robust estimators (LS and PACE) after removing the outliers. It is interesting to note that on this "clean" data set, the PACE and ROB estimators are qualitatively similar (see Figures 11 and 12).

We further compare these fits in terms of their prediction ability by randomly splitting the data into a training set and a test set (with 80% and 20% of the curves, respectively). We estimate the mean and covariance functions using the training set,

(a) First eigenfunctions (b) Second eigenfunctions

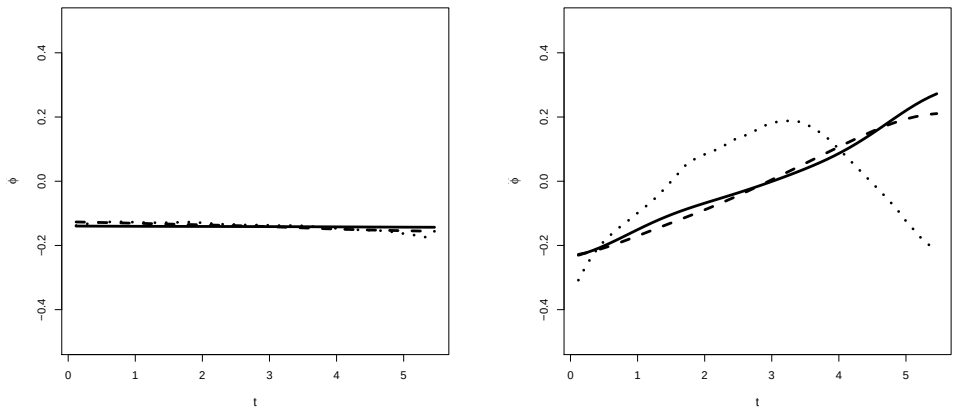



Figure 10: Estimated eigenfunctions associated with the two largest eigenvalues of the corresponding covariance function estimate. Robust estimates (ROB) are displayed with solid lines, their non-robust alternatives (LS) use dashed lines, while PACE is shown with dotted curves.

(a) ROB (b) LS (c) PACE

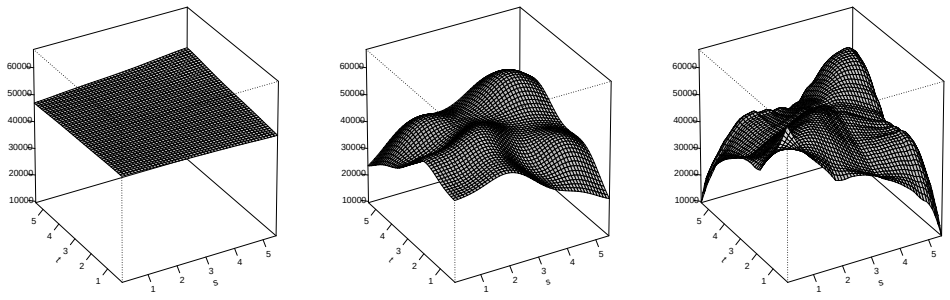



Figure 11: Estimated covariance functions with LS and PACE after removing trajectories that were flagged as possible outliers together with the robust estimated covariance function using all the data.

and use them to obtain predicted curves for the 20% held-out curves in the test set. Figure 13 below displays four curves in the test set (shown in gray), with the 3

(a) First eigenfunctions (b) Second eigenfunctions

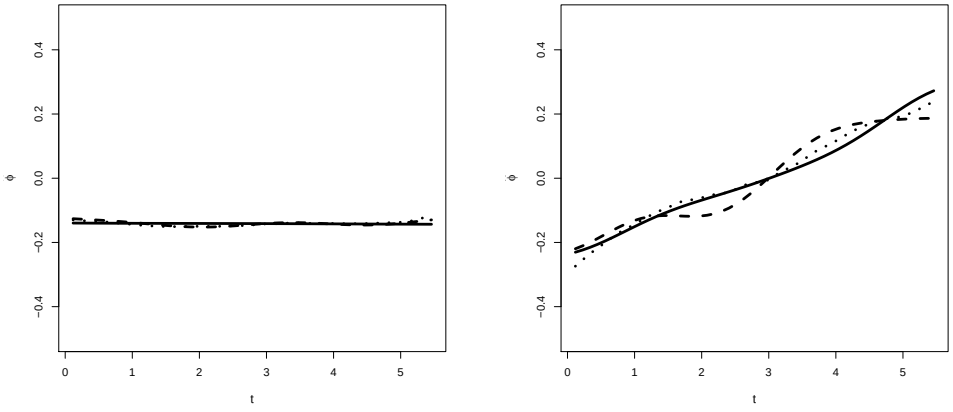
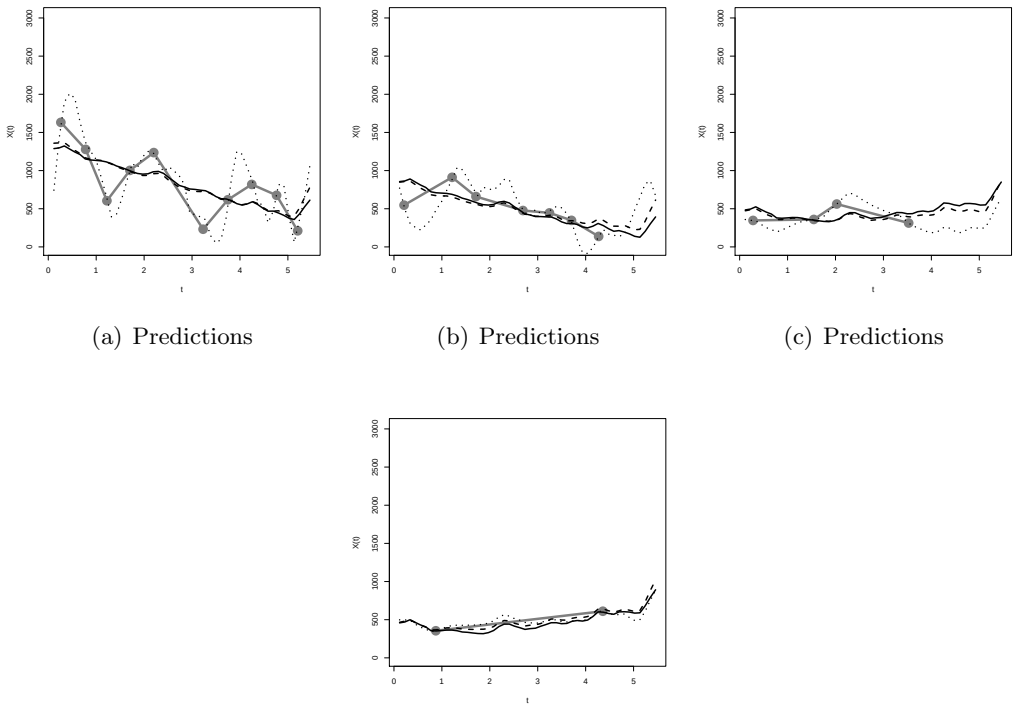



Figure 12: Estimated eigenfunctions after removing trajectories that were flagged as possible outliers. The robust estimates (ROB) are displayed with solid lines, the non-robust version (LS) uses dashed lines, while PACE is shown with dotted curves.

predicted trajectories.

# 6 Conclusion

We propose a novel robust functional principal components analysis (FPCA) method that is appropriate for applications in which only a few observations per unit or trajectory are available. Such longitudinal data sets with few points per curve (possibly recorded at irregular intervals) are relatively common in applications, and it is often natural to assume an underlying functional structure (of smooth trajectories, for example). Although our motivation was the development of a robust FPCA approach, the proposed method can easily be extended to obtain an alternative to PACE (Yao *et al.* [56]) for cases where no atypical observations are present in the data. Our method only assumes that the underlying random process has an elliptical distribution, and thus it is applicable even with heavy-tailed data (for example, without finite moments). Our simulation studies confirm that the robust version of this approach remains informative when the data contains outliers (which need not be extreme values), and behave similarly to the non-robust alternatives when the data are clean. Furthermore, in both our numerical experiments and the example the non-robust variant of our proposal compares favourably to the existing



(a) Predictions (b) Predictions (c) Predictions

(d) Predictions

Figure 13: Predicted trajectories for four curves in the test set. The predictions based on the ROB estimator are shown with solid lines, the non-robust ones based on LS use dashed lines, while those based on PACE are shown with dotted lines.

methods in the literature. Our methodology could, in principle, also be used to derive robust estimators for functional principal components regression models (see Febrero-Bande *et al.* [17] for a recent review) when only a few observations per curve are available. We will explore this idea in future work.

## Acknowledgements

The authors wish to thank two anonymous referees for valuable comments which led to an improved version of the original paper. They also thank Prof. Jane-Ling Wang for helpful discussions during the early stages of our work. This research was partially supported by Grants 20020170100022BA from the Universidad de Buenos Aires and PICT 2018-00740 from ANPCYT at Buenos Aires, Argentina and also by

the Spanish Project MTM2016-76969P from the Ministry of Economy, Industry and Competitiveness (MINECO/AEI/FEDER, UE) (Graciela Boente) and by Discovery Grant RGPIN-2016-04288 of the Natural Sciences and Engineering Research Council of Canada (M. Salibián Barrera).

# 7 Appendix - Proof of Proposition 3.1

Although the proof of Proposition 3.1 is immediate when $\Gamma$ has finite rank, we include it here for completeness. The infinite-dimensional case is proved using the representation $X \sim \mu + S\,V$ for elliptical random elements (Boente *et al.* [7]), where $S \geq 0$ is a random variable independent from the zero-mean Gaussian random element $V$

**Proof of Proposition 3.1.** First note that it is sufficient to prove the result when $\mu = 0$. Specifically, let $\widetilde{X} = X - \mu \sim \mathcal{E}(0, \Gamma, \varphi)$, $\mathbf{X}_m = (X(t_1), \ldots, X(t_m))^{\mathrm{T}}$ and $\widetilde{\mathbf{X}}_m = (\widetilde{X}(t_1), \ldots, \widetilde{X}(t_m))^{\mathrm{T}} = \mathbf{X}_m - (\mu(t_1), \ldots, \mu(t_m))^{\mathrm{T}}$. It will then follow that $\widetilde{\mathbf{X}}_m$ has a multivariate elliptical distribution with location vector $\mathbf{0}$, and hence that $\mathbf{X}_m$ has a multivariate elliptical distribution with location $(\mu(t_1), \ldots, \mu(t_m))^{\mathrm{T}}$ and the same scatter matrix as $\widetilde{\mathbf{X}}_m$.

In what follows assume that $\mu = 0$. Consider first the case where there are only finitely many non-zero eigenvalues, $\lambda_1 \geq \lambda_2 \geq \cdots \geq \lambda_q$, $\lambda_\ell = 0$ for $\ell > p$, and let $\phi_1$, $\ldots$, $\phi_q$ be the corresponding eigenfunctions. Define the operator $A : L^2(\mathcal{I}) \to \mathbb{R}^q$ as $Af = (\langle f, \phi_1 \rangle, \ldots, \langle f, \phi_q \rangle)^{\mathrm{T}}$. This operator is linear, and also bounded since by the Cauchy-Schwartz inequality we have

$$\|Af\|^2_{\mathbb{R}^p} = \sum_{i=1}^{q} \left( \int f(t)\phi_i(t)dt \right)^2 \leq \sum_{i=1}^{q} \left( \|f\|_{L^2} \|\phi_i\|_{L^2} \right)^2 = q\,\|f\|^2_{L^2}\,.$$

Using that $A$ is a linear and bounded operator and the definition of elliptical elements in $L^2(\mathcal{I})$, we have that $AX$ is an elliptical random vector. Furthermore, using (2), we have

$$AX = (\langle X, \phi_1 \rangle, \langle X, \phi_2 \rangle, \cdots, \langle X, \phi_q \rangle)^{\mathrm{T}} = (\xi_1, \xi_2, \cdots, \xi_q)^{\mathrm{T}}\,.$$

Thus, $\boldsymbol{\xi} = (\xi_1, \xi_2, \cdots, \xi_q)^{\mathrm{T}}$ is an elliptical random vector $\mathcal{E}_q(\mathbf{0}_q, A\Gamma A^*, \varphi)$. It is easy to see that $A\Gamma A^* = \mathrm{diag}(\lambda_1, \ldots, \lambda_q)$, since $A^*\mathbf{u} = \sum_{j=1}^{q} u_j \phi_j$, for any $\mathbf{u} \in \mathbb{R}^q$. Hence $\boldsymbol{\xi} \sim \mathcal{E}_q(\mathbf{0}_q, \Lambda_q, \varphi)$, where $\Lambda_q = \mathrm{diag}(\lambda_1, \ldots, \lambda_q)$. Moreover, noticing that for any $s \geq 1$ and $\ell_1 \leq \ell_2 \leq \cdots \leq \ell_s$, such that $\ell_1 > q$, $(\langle X, \phi_{\ell_1} \rangle, \ldots, \langle X, \phi_{\ell_s} \rangle)$ has also an elliptical distribution with location zero and null scatter matrix, that is, it equals

$\mathbf{0}_s$ with probability one, we get that $X \sim \sum_{j=1}^{q} \xi_j \phi_j$. Let $\mathbf{B} \in \mathbb{R}^{m\times q}$ with $(i,j)$-th entry $\mathbf{B}_{ij} = \phi_j(t_i)$, $1 \le i \le m$, $1 \le j \le q$. Then,

$$\mathbf{X}_m = (X(t_1), X(t_2), \cdots, X(t_m))^{\mathrm{T}} = \mathbf{B}\,\boldsymbol{\xi} \sim \mathcal{E}_m(\mathbf{0}_m, \mathbf{B}\Lambda_q\mathbf{B}^{\mathrm{T}}, \varphi)\,.$$

Finally, note that the $(s,\ell)$ element of $\mathbf{B}\Lambda_q\mathbf{B}^{\mathrm{T}}$ equals $\sum_{j=1}^{q} \lambda_j\phi_j(t_s)\phi_j(t_\ell) = \gamma(t_s,t_\ell)$, which concludes the proof of (a) for finite rank processes.

If infinitely many $\lambda_i$'s are non-zero, then using Proposition 2.1 in Boente *et al.* [7] we have $X \sim S\,V$ where $S \ge 0$ is a random variable independent of the Gaussian element $V$. Hence

$$\mathbf{X}_m \,=\, (X(t_1), X(t_2), \cdots, X(t_m))^{\mathrm{T}} \,=\, S\,\mathbf{V}_p\,,$$

where $S \ge 0$ is independent of $\mathbf{V}_p = (V(t_1), \ldots, V(t_m))^{\mathrm{T}}$. Note that the covariance operator of $V$ is a scalar multiple of $\Gamma$, without loss of generality, we may assume that $\Gamma_V = \Gamma$. The fact that $V$ is a Gaussian process with continuous covariance kernel $\gamma(s,t)$ entails that $\mathbf{V}_p$ is an $m-$variate normally distributed vector. Effectively, Theorem 1.5 in Bosq [8] implies that

$$\lim_{p\to\infty} \sup_{t\in\mathcal{I}} \mathbb{E}\left(V(t) - \sum_{\ell=1}^{p} \eta_\ell\,\phi_\ell(t)\right)^2 = 0\,,$$

where $\eta_\ell = \langle V, \phi_\ell\rangle \sim N(0,\lambda_\ell)$ are independent. Let $V_p(t) = \sum_{\ell=1}^{p} \eta_\ell\,\phi_\ell(t)$, then $\mathbf{V}_{p,m} = (V_p(t_1), \ldots, V_p(t_m))^{\mathrm{T}} \xrightarrow{D} \mathbf{V}_m = (V(t_1), \ldots, V(t_m))^{\mathrm{T}}$, as $p \to \infty$. Note that $\mathbf{V}_{p,m}$ has a multivariate normal distribution $N_m(\mathbf{0}_m, \boldsymbol{\Sigma}_{p,m})$ with $(s,\ell)$ element of $\boldsymbol{\Sigma}_{p,m}$ equal to $\sum_{j=1}^{p} \lambda_j\ \phi_j(t_s)\ \phi_j(t_\ell)$. Then, taking into account that $\sum_{\ell\ge1} \lambda_\ell\phi_\ell^2(t_i) = \gamma(t_i,t_i) < \infty$, we obtain easily that $\mathbf{V}_m \sim N(0, \boldsymbol{\Sigma}_{\mathbf{V}_m})$, where the $(s,\ell)$ element of $\boldsymbol{\Sigma}_{\mathbf{V}_m}$ equals $\gamma(t_s,t_\ell)$. Hence, $\mathbf{X}_m$ has an elliptical distribution. Taking into account that $\Gamma_V = \Gamma$, we obtain that $\mathbf{X}_m \sim \mathcal{E}_m(\mathbf{0}_m, \boldsymbol{\Sigma}, \varphi)$, where the $(s,\ell)-$th element of $\boldsymbol{\Sigma}$ equals $\gamma(t_s,t_\ell)$, concluding the proof of (a).

Part (b) follows immediately from (a).

To prove (c), note again that it is enough to obtain the result when $\mu = 0$. Let us first consider the finite-rank case, when $\lambda_\ell = 0$ for $\ell > q$. From (a), we have $\boldsymbol{\xi} = (\xi_1, \xi_2, \cdots, \xi_q)^{\mathrm{T}} \sim \mathcal{E}_q(\mathbf{0}_q, \mathrm{diag}(\lambda_1, \ldots, \lambda_q), \varphi)$ and $\mathbf{X}_m = (X(t_1), \cdots, X(t_m))^{\mathrm{T}} = \mathbf{B}\,\boldsymbol{\xi}$. Hence,

$$\mathbf{W} = (\xi_k, X(t_1), X(t_2), \cdots, X(t_m))^{\mathrm{T}} = \begin{pmatrix} \mathbf{e}_k^{\mathrm{T}} \\ \mathbf{B} \end{pmatrix} \boldsymbol{\xi} = \mathbf{M}\boldsymbol{\xi}$$

with $\mathbf{e}_k$ the $k-$th canonical vector in $\mathbb{R}^q$. Thus, $\mathbf{W} \sim \mathcal{E}_{q+1}(\mathbf{0}_{q+1}, \mathbf{\Sigma}_{\mathbf{W}}, \varphi)$, where $\mathbf{\Sigma}_{\mathbf{W}} = \mathbf{M}\ \mathrm{diag}(\lambda_1, \ldots, \lambda_q)\ \mathbf{M}^{\mathrm{T}}$ is given by

$$\mathbf{\Sigma}_{\mathbf{W}} = \begin{pmatrix} \lambda_k & \lambda_k \boldsymbol{\phi}_k^{\mathrm{T}} \\ \lambda_k\ \boldsymbol{\phi}_k & \mathbf{\Sigma}_{\mathbf{X}_m} \end{pmatrix} \tag{13}$$

with $\mathbf{\Sigma}_{\mathbf{X}_m}$ and $\boldsymbol{\phi}_k$ as in the statement of the Proposition. The conclusion follows now immediately from properties of the conditional distribution of elliptical distributions, see, for instance, Corollary 8 in Frahm [21], where an expression for the characteristic generator is also given.

When $\Gamma$ does not have finite rank, as in the proof of (a), from Proposition 2.1 in Boente *et al.* [7] we conclude that $X \sim S\ V$, where $S \geq 0$ is a random variable independent of the Gaussian element $V$ and the covariance operator of $V$ equals $\Gamma$. Then,

$$\mathbf{W} = (\xi_k, X(t_1), X(t_2), \cdots, X(t_m))^{\mathrm{T}} \ = \ S\ (\eta_k, V(t_1), V(t_2), \cdots, V(t_m))^{\mathrm{T}}$$

with $\eta_k = \langle V, \phi_k \rangle \sim N(0, \lambda_k)$. Note that the fact that $\eta_k \sim N(0, \lambda_k)$ entails that $\xi_k = S\,\eta_k$ is finite almost surely. Moreover, with a similar argument as in the proof of part (a) and using the continuity of $\gamma$ it is easy to see that the random vector $\mathbf{V} = (\eta_k, V(t_1), V(t_2), \cdots, V(t_m))$ is normally distributed with zero mean and covariance matrix given in (13). Hence $\mathbf{W} \sim \mathcal{E}_{p+1}(\mathbf{0}_{p+1}, \mathbf{\Sigma}_{\mathbf{W}}, \varphi)$ and the result follows again from the properties of the multivariate elliptical distributions. $\square$

# References


[1] Bali, J. L. and Boente, G. (2009). Principal points and elliptical distributions from the multivariate setting to the functional case. *Statistics and Probability Letters*, **79**, 1858-1865.

[2] Bali, J. L., Boente, G., Tyler, D. and Wang, J. L. (2011). Robust functional principal components: a projection-pursuit approach. *Annals of Statistics*, **39**, 2852-2882.

[3] Billor, N., Hadi, A. and Velleman, P. (2000) BACON: blocked adaptive computationally efficient outlier nominators. *Computational Statistics & Data Analysis*, **34**, 279-298.

[4] Boente, G. and Fraiman, R. (1989). Robust nonparametric regression estimation. *Journal of Multivariate Analysis*, **29**, 180-198.

[5] Boente, G., Rodriguez, D. and Sued, M. (2019). The spatial sign covariance operator: Asymptotic results and applications. *Journal of Multivariate Analysis*. **170**, 115-128.

[6] Boente, G. and Salibián-Barrera, M. (2015). $S-$estimators for functional principal component analysis. *Journal of the American Statistical Association*, **110**, 1100-1111.

[7] Boente, G., Salibián-Barrera, M. and Tyler, D. E. (2014). A characterization of elliptical distributions and some optimality properties of principal components for functional data. *Journal of Multivariate Analysis*, **131**, 254-264.

[8] Bosq, D. (2000). *Linear Processes in Function Spaces*. Springer, New York

[9] Cardot, H., Cénac, P. and Zitt, P.. (2013). Efficient and fast estimation of the geometric median in Hilbert spaces with an averaged stochastic gradient algorithm, *Bernoulli*, **19**, 18-431.

[10] Cardot, H. and Godichon-Baggioni, A. (2017). Fast estimation of the median covariation matrix with application to online robust principal components analysis. *TEST*, **26**, 461-480.

[11] Cevallos-Valdiviezo, H. (2016). *On methods for prediction based on complex data with missing values and robust principal component analysis*, PhD thesis, Ghent University (supervisors Van Aelst S. and Van den Poel, D.)

[12] Chen, Y., Carroll, C., Dai, X., Fan, J., Hadjipantelis, P.Z., Han, K., Ji, H., Müller, H.G. and Wang, J.L. (2020). *fdapace: Functional Data Analysis and Empirical Dynamics. R package version 0.5.2.* `https://CRAN.R-project.org/package=fdapace`.

[13] Cuevas, A. (2014). A partial overview of the theory of statistics with functional data. *Journal of Statistical Planning and Inference*, **147**, 1-23.

[14] Cuevas, A., Febrero,M. and Fraiman, R.. (2007). Robust estimation and classification for functional data via projection-based depth notions, *Computational Statistics*, **22**, 481-496.

[15] Febrero, M., Galeano, P. and Gonzalez-Manteiga, W. (2007). A functional analysis of NOx levels: location and scale estimation and outlier detection. *Computational Statistics*, **22**, 411-427.

[16] Febrero, M., Galeano, P. and Gonzalez-Manteiga, W. (2008). Outlier detection in functional data by depth measures, with application to identify abnormal NOx levels. *Environmetrics*, **19**, 331-345.

[17] Febrero-Bande, M.; Galeano, P. and González-Manteiga, W. (2017). Functional principal component regression and functional partial least-squares regression: An overview and a comparative study. *International Statistical Review*, **85**, 61-83.

[18] Ferraty, F. and Romain, Y. (2010). *The Oxford Handbook of Functional Data Analysis*, Oxford University Press.

[19] Ferraty, F. and Vieu, Ph. (2006). *Nonparametric Functional data analysis: Theory and Practice*. Springer Series in Statistics, Springer, New York.

[20] Fischl, M.A., Ribaudo, H.J., Collier, A.C., Erice, A., Giuliano, M., Dehlinger, M., Eron, J.J. Jr., Saag, M.S., Hammer, S.M., Vella, S., Morse, G.D., Feinberg, J.E., Demeter, L.M., Eshleman, S.H. and Adult AIDS Clinical Trials Group 388 Study Team (2003). A randomized trial of 2 different 4-drug antiretroviral regimens versus a 3-drug regimen, in Advanced Human Immunodeficiency Virus disease. *Journal of Infectious Diseases*, **188**, 625-634.

[21] Frahm, G. (2004). *Generalized Elliptical Distributions: Theory and Applications*. PhD. thesis from the University of Köln, Germany.

[22] Fraiman, R. and Muñiz, G. (2001). Trimmed means for functional data. *Test*, **10**, 419-440.

[23] Gervini, D. (2008). Robust functional estimation using the median and spherical principal components. *Biometrika*, **95**, 587-600.

[24] Gervini, D. (2009). Detecting and handling outlying trajectories in irregularly sampled functional datasets. *Annals of Applied Statististics*, **3**, 1758-1775.

[25] Goia, A. and Vieu, P. (2016). An introduction to recent advances in high/infinite-dimensional statistics. *Journal of Multivariate Analysis*, **146**, 1-6.

[26] Hall, P. and Horowitz, J. L. (2007). Methodology and convergence rates for functional linear regression. *Annals of Statistics*, **35**, 70-91.

[27] Härdle (1990). *Applied Nonparametric Regression*. Econometric Society Monographs, 19, Cambridge University Press, Cambridge.

[28] Härdle, W. and Tsybakov, B. (1988). Robust nonparametric regression with simultaneous scale curve estimation. *Annals of Statistics*, **16**, 120-135.

[29] Horváth, L. and Kokoszka, P. (2012). *Inference for functional data with applications*. Springer, New York.

[30] Hsing, T. and Eubank, R. (2015). *Theoretical Foundations of Functional Data Analysis, with an Introduction to Linear Operators*, Wiley, New York.

[31] Hubert, M., Rousseeuw, P. and Branden, K. (2005) ROBPCA: a new approach to robust principal component analysis. *Technometrics*, **47**, 64-79

[32] Hubert M., Rousseeuw P. and Segaert P. (2015). Multivariate functional outlier detection. *Statistical Methods and Applications*, **24**, 177-202.

[33] Hubert, M. and Vandervieren, E. (2008). An adjusted boxplot for skewed distributions. *Computational Statistics & Data Analysis*, **52**, 5186-5201.

[34] Hyndman, R. and Shang, H. (2010). Rainbow plots, bagplots, and boxplots for functional data. *Journal of Computational and Graphical Statistics*, **19**, 29-45.

[35] Hyndman, R. J. and Ullah, S. (2007). Robust forecasting of mortality and fertility rates: A functional data approach. *Computational Statistics and Data Analysis*, **51**, 4942-4956.

[36] James, G., Hastie, T. and Sugar, C. (2000). Principal Component Models for Sparse Functional Data. *Biometrika*, **87**(3), 587-602.

[37] Kraus, D. and Panaretos, V. M. (2012). Dispersion operators and resistant second-order functional data analysis. *Biometrika*, **99**, 813-832.

[38] Lee, S., Shin, H. and Billor, N. (2013). $M$-type smoothing spline estimators for principal functions. *Computational Statistics and Data Analysis*, **66**, 89-100.

[39] Li, Y. and Hsing, T. (2010). Uniform convergence rates for nonparametric regression and principal component analysis in functional/longitudinal data. *Annals of Statistics*, **38**, 3321-3351.

[40] Locantore, N., Marron, J., Simpson, D., Tripoli, N., Zhang, J. and Cohen, K. (1999). Robust principal components for functional data, *Test*, **8**, 1-28.

[41] López-Pintado, S. and Romo, J. (2007). Depth-based inference for functional data. *Computational Statistics & Data Analysis*, **51**, 4957-4968.

[42] Maronna, R., Martin, R., Yohai, V. and Salibián-Barrera, M. (2019). *Robust Statistics: Theory and Methods (with R)*. Wiley, New York.

[43] Maronna, R. (2019). Robust functional principal components for irregularly spaced longitudinal data. In press in *Statistical Papers*. `https://doi.org/10.1007/s00362-019-01147-2`

[44] Oh, H-S., Nychka, D.W. and Lee, T.C.M. (2007). The role of pseudo data for robust smoothing with applications to wavelet regression. *Biometrika*, **94**, 893-904.

[45] Park, J.G. and Wu, H. (2006). Backfitting and local likelihood methods for non-parametric mixed-effects models with longitudinal data. *Journal of Statistical Planning and Inference*, **136**, 3760-3782.

[46] R Core Team (2020). R: A language and environment for statistical computing. R Foundation for Statistical Computing, Vienna, Austria. `URL:https://www.R-project.org/`.

[47] Ramsay, J. O. and Silverman, B. W. (2005). *Functional Data Analysis*, 2nd edition. Springer, New York.

[48] Sawant, P., Billor, N. and Shin, H. (2012). Functional outlier detection with robust functional principal component analysis. *Computational Statistics*, **27**, 83-102.

[49] Schauberger, G. and Tutz, G. (2020). *catdata: Categorical Data. R package version 1.2.2.* `https://CRAN.R-project.org/package=catdata`

[50] Sinova, B., Gonzalez-Rodriguez, G. and Van Aelst, S. (2018). M-estimators of location for functional data. *Bernoulli*, **24**, 2328-2357.

[51] Staniswalis, J. G. and Lee, J. J. (1998). Nonparametric regression analysis of longitudinal data. *Journal of the American Statistical Association*, **93**, 1403-1418.

[52] Sun, Y. and Genton, M. G. (2011). Functional boxplots. *Journal of Computational and Graphical Statistics*, **20**, 316-334.

[53] Wang, J.L., Chiou, J., Müller, H.G. (2016). Functional Data Analysis. *Annual Review of Statistics and Its Application*, **3**, 257-295.

[54] Welsh, A.H. (1996). Robust estimation of smooth regression and spread functions and their derivatives. *Statistica Sinica*, **6**, 347-366.

[55] Wood, S. (2017). *Generalized Additive Models: An Introduction with R*. CRC Press, Taylor and Francis, Boca Raton.

[56] Yao, F., Müller, H.G. and Wang, J.L. (2005). Functional data analysis for sparse longitudinal data. *Journal of the American Statistical Association*, **100**, 577-590.

[57] Zeger, S.L. and Diggle, P.J. (1994). Semiparametric models for longitudinal data with application to CD4 cell numbers in HIV seroconverters. *Biometrics*, **50**, 689-699.